1980

Surface effect ship heave control using a linear regulator design.

Everett, Dwight H.

Monterey, California. Naval Postgraduate School

NAVAL POSTGRADUATE SCHOOL
Monterey, California

THESIS

SURFACE EFFECT SHIP HEAVE CONTROL
USING A LINEAR REGULATOR DESIGN

by

Dwight H. Everett

March 1980

Thesis Advisor: A. Gerba, Jr.

SECURITY CLASSIFICATION OF THIS PAGE (When Data Entered)

REPORT DOCUMENTATION PAGE		READ INSTRUCTIONS BEFORE COMPLETING FORM
1. REPORT NUMBER	2. GOVT ACCESSION NO.	3. RECIPIENT'S CATALOG NUMBER
4. TITLE (and Subtitle) Surface Effect Ship Heave Control Using A Linear Regulator Design		5. TYPE OF REPORT & PERIOD COVERED Master's Thesis; March 1980 6. PERFORMING ORG. REPORT NUMBER
7. AUTHOR(s) Dwight H. Everett		8. CONTRACT OR GRANT NUMBER(s)
9. PERFORMING ORGANIZATION NAME AND ADDRESS Naval Postgraduate School Monterey, California 93940		10. PROGRAM ELEMENT, PROJECT, TASK AREA & WORK UNIT NUMBERS
11. CONTROLLING OFFICE NAME AND ADDRESS Naval Postgraduate School Monterey, California 93940		12. REPORT DATE March 1980 13. NUMBER OF PAGES 105
14. MONITORING AGENCY NAME & ADDRESS(if different from Controlling Office)		15. SECURITY CLASS. (of this report) UNCLASSIFIED 15a. DECLASSIFICATION/DOWNGRADING SCHEDULE

16. DISTRIBUTION STATEMENT (of this Report)

Approved for public release; distribution unlimited

17. DISTRIBUTION STATEMENT (of the abstract entered in Block 20, if different from Report)

18. SUPPLEMENTARY NOTES

19. KEY WORDS (Continue on reverse side if necessary and identify by block number)

Optimal Control
Vertical Plane Motion
Linear Regulator Technique
XR-3 Surface Effect Ship

20. ABSTRACT (Continue on reverse side if necessary and identify by block number)

A control system was designed to attenuate vertical accelerations for the XR-3 captured air bubble type surface effect ship using linear regulator techniques applied to the simplified nonlinear equations of motion. A pressure lift-only model was used to represent the craft vertical heave motion and was linearized around the steady state operating point. Model validation was obtained through analysis of the frequency spectrum. State variable feedback was used to determine a set of optimal control gains that would

DD FORM 1 JAN 73 1473 EDITION OF 1 NOV 65 IS OBSOLETE
S/N 0102-014-6601
(Page 1)

SECURITY CLASSIFICATION OF THIS PAGE (When Data Entered)

reduce the magnitude of the heave acceleration during operation under simulated sea input conditions.

Approved for public release; distribution unlimited

SURFACE EFFECT SHIP HEAVE CONTROL USING A LINEAR REGULATOR DESIGN

by

Dwight H. Everett
Lieutenant, United States Navy
B.S.E.E., University of Washington, 1974

Submitted in partial fulfillment of the
requirements for the degree of

MASTER OF SCIENCE IN ELECTRICAL ENGINEERING

from the

NAVAL POSTGRADUATE SCHOOL
March 1980

ABSTRACT

A control system was designed to attenuate vertical accelerations for the XR-3 captured air bubble type surface effect ship using linear regulator techniques applied to the simplified nonlinear equations of motion. A pressure lift-only model was used to represent the craft vertical heave motion and was linearized around the steady state operating point. Model validation was obtained through analysis of the frequency spectrum. State variable feedback was used to determine a set of optimal control gains that would reduce the magnitude of the heave acceleration during operation under simulated sea input conditions.

TABLE OF CONTENTS

I. INTRODUCTION- - - - - - - - - - - - - - - - - - - 7

II. PRESENTATION OF THE SYSTEM- - - - - - - - - - - 10

A. EQUATIONS OF MOTION - - - - - - - - - - - - - 11

B. LINEAR MODEL- - - - - - - - - - - - - - - - - 18

1. Transfer Function Development - - - - - - 18

2. State Equation Development- - - - - - - - 26

3. The Characteristic Equation - - - - - - - 30

III. VERIFICATION OF THE MODEL - - - - - - - - - - - 36

A. LINEAR AND NONLINEAR SYSTEM VALIDATION- - - 36

IV. THE CONTROL LAW - - - - - - - - - - - - - - - - 44

A. LINEAR REGULATOR DESIGN APPROACH- - - - - - 44

B. SENSITIVITY AND STABILITY - - - - - - - - - 47

1. The Characteristic Equation For Feedback Control Applied- - - - - - - - 51

2. Root Locus- - - - - - - - - - - - - - - - 53

3. Routh Criterion - - - - - - - - - - - - - 62

V. CONCLUSION - - - - - - - - - - - - - - - - - - 65

VI. RECOMMENDATIONS FOR FURTHER STUDY - - - - - - - 67

APPENDIX A- 69

APPENDIX B- 78

APPENDIX C- 83

APPENDIX D- 91

APPENDIX E- 94

LIST OF REFERENCES- - - - - - - - - - - - - - - - - 104

INITIAL DISTRIBUTION LIST - - - - - - - - - - - - - 105

ACKNOWLEDGEMENTS

I would like to take this opportunity to express my appreciation to Professor Alex Gerba for his sustained patience and insight. The guidance provided from Professor Gerba and Professor Thaler was invaluable in the preparation of this thesis. To my wife and family go a very special thanks for their understanding and sacrifice.

I. INTRODUCTION

An important design consideration for the high speed captured air bubble type surface effect ship is the vertical acceleration associated with operation in a random ocean environment [Ref. 1]. The vertical motion, heave, is caused by waves changing the volume of the plenum producing pressure variations that result in vertical craft accelerations.

Studies of conventional hull ships show that the strongest vertical plane accelerations are experienced at encounter frequencies close to the ship's natural frequency. Reference 2 states that "The most severe and objectionable motions (wet decks, slamming, high accelerations) result from the responses to the components that are near synchronism with the ship's natural pitching and heaving periods". Encounter frequency is a function of wave frequency, craft speed and direction. Since most of the weight of the surface effect ship is supported by a bubble of air, large accelerations can occur that affect habitability and sea keeping ability while operating in high seas.

Methods of attenuating vertical motion have been the subject of past studies. A conventional design by Rohr Marine Inc. [Ref. 3] utilized accelerometer output to monitor vertical motion variations. These signals are passed through compensation circuits, filtered and applied to actuators

which control air flow rates into the plenum. State variable techniques are applied to describe the system and control functions. The physical constraints of the actuators are considered with regard to their inherent nonlinearities and limitations. The sea input is modeled using a wave height power spectral density procedure.

Through the use of a towing tank model and data gathered from the 100B test craft, an investigation was conducted to measure the characteristic response of the SES while operating in an actual sea state environment [Ref. 4]. The model was subjected to simulated sea state inputs of various severity in an effort to establish the linear characteristics of the vertical motion and determine the damped natural frequency of response. A series of curves showing response amplitude for both C.G. accelerations and pitch angle versus encounter frequency were developed for a range of speed and sea state operation.

In Ref. 1, the frequency response approach was used in an analysis which examined the effects of changing plenum air flow rates on center of gravity accelerations using the six degree of freedom simulation program of the XR-3 [Ref. 5]. This study developed a linear simplified model in close agreement with the 6 D.O.F. model and in addition used significantly less computer time.

In Ref. 6, Boggio conducted a study on the effect of the use of a flexible membrane in the plenum chamber itself. Using the loads and motions program for the XR-3, the study

reduced computation time through the inclusion of pressure rate and volume rate equations. Membrane insertion served to effectively reduce the magnitude of pressure variations in the plenum thereby attenuating vertical motions.

Grant [Ref. 7] used simple models for the control devices applied to the loads and motions program of the 100B SES craft. From monitored plenum pressure variations and heave accelerations, control signals were developed by filter design methods, to vary the fan speed and vent louver openings in order to reduce the vertical accelerations and pitch motion.

This thesis applies the linear regulator design technique to determine a set of optimal state feedback gains to control the air flow rate. The equations of motion used in the design were derived from a simplified pressure lift only model linearized around the steady state operating point. Design results were evaluated using both the linear and nonlinear models.

II. PRESENTATION OF THE SYSTEM

Two major forces which support the weight of the surface effect ship are the buoyancy and plenum pressure forces. The buoyancy forces (F_L) are exerted on the craft by displacement of water by the underwater volume of the rigid sidewalls. The plenum pressure lift force (F_P) is exerted on the craft by the captured cushion of air. Flexible bow and stern seals along with the rigid sidewalls and lift fans form the captured air bubble. Relative contributions to craft vertical plane motion by F_L and F_P depend upon the encounter frequency (ω_e). At low frequencies, F_L responds to the rise and fall of the sea. At high ω_e, F_L attenuates because incremental volume changes of the immersed hull are reduced. The F_P force responds inversly to changes in plenum volume (V_B) according to the adiabatic law of pressure variations within the plenum chamber [Ref. 1]. Volumetric changes in the plenum depend upon the sea state and encounter frequency. As is shown in Ref. 1, the effect of the volume changes produces an increase in the F_P force as the encounter frequency is increased.

In the system developed in this study, the buoyancy terms have been omitted in an effort to simplify the system further. This simplified model is referred to as the "pressure lift only" system. Transfer functions of acceleration, volumetric

plenum air mass to input waveheight and system state equations were developed from the linearized form of the pressure lift only system.

The basic assumptions which form the basis for the pressure lift only model are presented below:

1. The center of pressure (C_p) is directly under the center of gravity (C.G.).
2. The sidewalls are of uniform cross section and are symmetrical about the C.G.
3. The effect of pitch moments on the vertical plane forces are neglected.
4. The only variable lift forces are those forces caused by changes in plenum pressure ($\overline{P}_b$).
5. The craft is at a constant speed.
6. The air leakage rate from the rear seal is constant.
7. The craft weight is supported by two component forces in the following approximate proportions;

   Sidewalls: 20% (fixed force)

   Captured Air Bubble: 80% (variable force)
8. Encounter frequencies of interest lie within the range of $17 < \omega_e < 100$ radians/sec.

A. EQUATIONS OF MOTION

The development of the nonlinear simplified model for vertical motion is presented in Ref. 1 and the block diagram appears in Appendix A. The development of the pressure lift only nonlinear model follows in a similar manner. The equations of motion differ in that the F_L force is considered constant.

The application of the given assumptions to the Newtonian Laws for vertical motion of a rigid body system leads to the following equations;

1) Orifice Leakage Rate

$$q_{out} = C_n A_1 \sqrt{\frac{2\bar{P}_b}{\rho_a}} \quad \frac{ft^3}{sec} \tag{2.A.1}$$

2) Fan Map Input Rate

$$q_{in} = n[Q_i(o) - K_q \bar{P}_b] \quad \frac{ft^3}{sec} \tag{2.A.2}$$

3) Absolute Plenum Pressure

$$P_b = P_a \left(\frac{M_b}{V_b \rho_a} \right)^{\gamma} \quad \frac{lbs}{ft^2} \tag{2.A.3}$$

4) Plenum Air Flow Rate

$$\dot{M}_b = \rho_a (q_{in} - q_{out}) \quad \frac{lbs}{sec} \tag{2.A.4}$$

5) Heave Acceleration

$$\ddot{Z} = \left(\frac{W}{M} - \frac{F_p}{M} - \frac{F_1}{M}\right) \quad \frac{ft}{sec}^2 \tag{2.A.5}$$

6) Heave Velocity

$$\dot{Z} = \int \ddot{Z}\, dt \quad \frac{ft}{sec} \tag{2.A.6}$$

7) Heave Displacement

$$Z = \int \dot{Z}\, dt \qquad \text{ft} \qquad (2.A.7)$$

8) Plenum Pressure Lift Force

$$F_p = A_b \overline{P}_b \qquad \text{lbs} \qquad (2.A.8)$$

9) Buoyancy Lift Force

$$F_l = [2A_s l_d \rho_g] \qquad \text{lbs} \qquad (2.A.9)$$

where l_d is steady state draft.

10) Plenum Gage Pressure

$$\overline{P}_b = (P_b - P_a) \qquad \frac{\text{lbs}}{\text{ft}^2} \qquad (2.A.10)$$

11) Draft

$$l_d = Z + Z_s \qquad \text{ft} \qquad (2.A.11)$$

The system parameters and constants are listed as follows:

1) Adiabatic Process Coefficient

$\gamma = 1.4$

2) Leakage Area

$A_l = Y_L Z_L = .438 \quad ft^2$

3) Leakage Orifice Coefficient

$C_n = .90$

4) Air Density

$\rho_a = .002378$

5) Atmospheric Pressure

$P_a = 2116$

6) Plenum Area

$A_b = 200 \quad ft^2$

7) Empty Plenum Volume

$V_n = 383 \quad ft^3$

8) Craft Weight

$W = 6007 \quad lbs$

9) Area of Each Immersed Sidewall

$A = 75/4 = 18.75 \quad ft^2$

10) Draft Initial Condition

$L_d(o) = .5 \quad ft$

11) Density of Water

$\rho = 1.99$

12) Gravity Acceleration Constant

$G = 32.174 \quad ft/sec^2$

13) Vertical Center of Gravity Location Above Keel Line

$Z_s = 2.5 \quad ft$

14) Number of Fans

$n = 5$

15) Steady State Fan Output

$Q_i(o) = 35 \quad ft^3/sec$

16) Fan Map Slope

$K_q = 1.0$

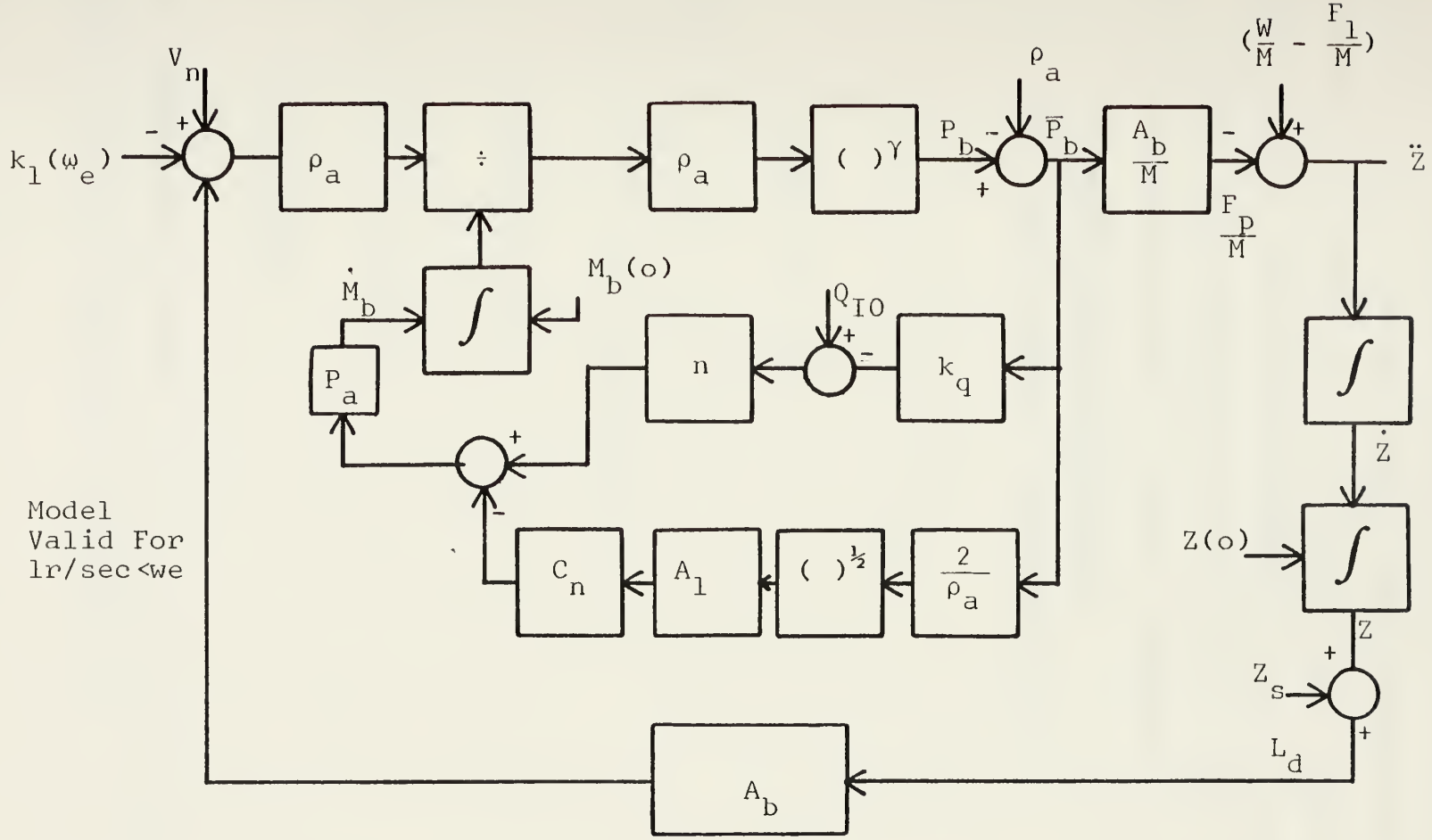

Figure 1

PRESSURE LIFT ONLY SCHEMATIC DIAGRAM

B. LINEAR MODEL

Prior to defining the system states, the non linear equations were linearized around their steady state operating conditions by application of a Taylor series expansion. The details of the linearization process is shown in Appendix A.

The resulting simplified pressure only signal flow graph for the linearized system is shown in Figure 2.

1. Transfer Function Development

The system graphical determinent is;

$$\Delta = 1 - (L_1 + L_2) + L_1 L_2 \qquad (2.B.1)$$

$$\Delta = 1 - (L_1 + L_2) \qquad (2.B.2)$$

where

$$L_1 = s^{-1}s^{-1}(-k_8)(-k_2)(k_3)(-k_4)$$

$$= -s^{-2}k_2k_3k_4k_8 \qquad (2.B.3)$$

$$L_2 = s^{-1}(k_7)(k_3)(-k_6)$$

$$= -s^{-1}k_3k_6k_7 \qquad (2.B.4)$$

The transmission gain from the control input to the acceleration output for calm water operation is;

LINEAR PRESSURE
LIFT ONLY SIGNAL
FLOW GRAPH

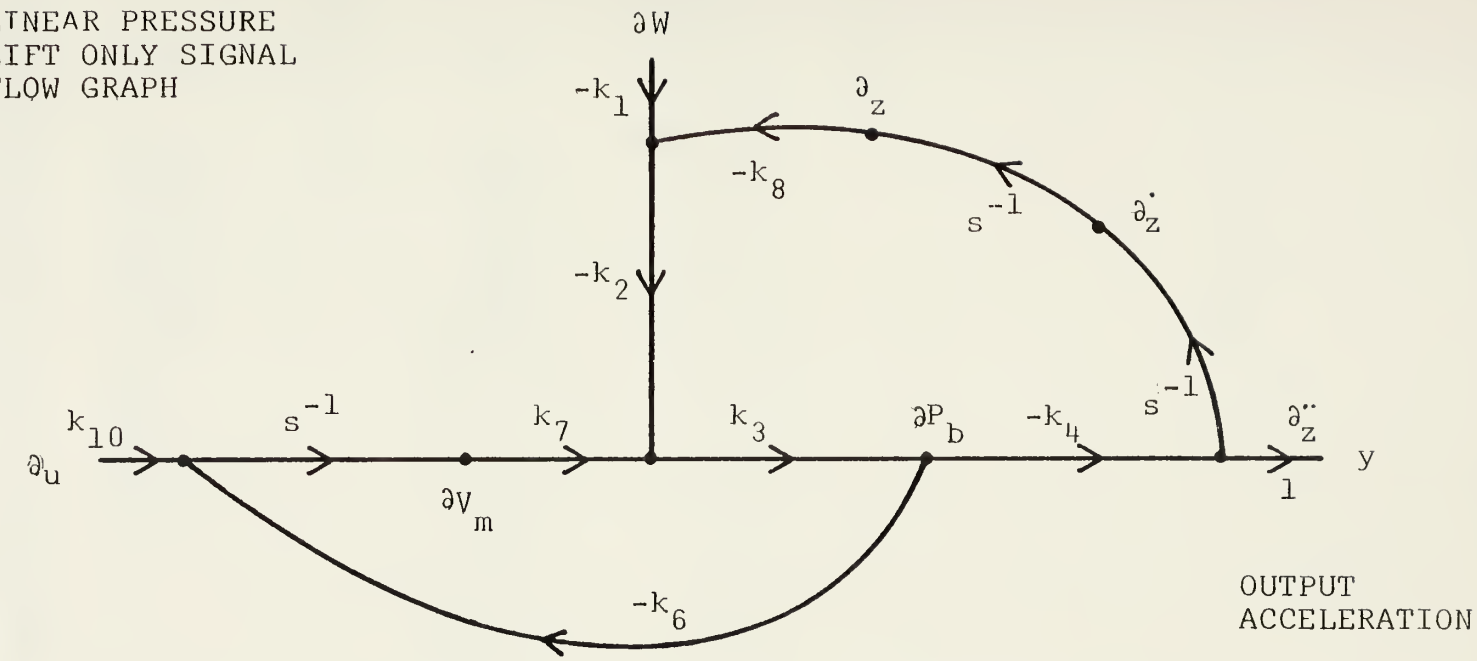

$$x = \begin{bmatrix} \partial_z \\ \dot{\partial}_z \\ \partial V_m \end{bmatrix} = \begin{bmatrix} x_1 \\ x_2 \\ x_3 \end{bmatrix}$$

$$y = \ddot{\partial}_z$$

NOTE: $-k_6$ is the coefficient for air leakage rate plus air influx rate set for calm water operating conditions

Figure 2

$$\ddot{\partial}_z = \frac{P_1 \Delta_1}{\Delta} \partial_u \qquad (2.B.5)$$

where

$$P_1 = -k_3 k_4 k_7 k_{10} s^{-1} \qquad (2.B.6)$$

and

$$\Delta_1 = 1 \qquad (2.B.7)$$

and

$$\partial_w = 0 \qquad (2.B.8)$$

Substituting equations (2.B.2), (2.B.6), (2.B.7) into equation (2.B.5) yields;

$$\ddot{\partial}_z = \frac{-k_3 k_4 k_7 k_{10} s^{-1}}{1-[-s^{-2} k_2 k_3 k_4 k_8)+(-s^{-1} k_3 k_6 k_7)]} \partial_u \qquad (2.B.9)$$

Reducing further;

$$\ddot{\partial}_z = \frac{-k_3 k_4 k_7 k_{10}}{s^2 + k_3 k_6 k_7 \, s + k_2 k_3 k_4 k_8} \partial_u \qquad (2.B.10)$$

The transmission gain from the sinusoidal sea generator input to the acceleration output with no control signal is;

$$\ddot{\partial}_z = \frac{P_2 \Delta_2}{\Delta} \partial_W \qquad (2.B.11)$$

where:

$$P_2 = -k_1k_2k_3k_4 \qquad (2,B.12)$$

and

$$\Delta_1 = 1 \qquad (2,B.13)$$

and

$$\partial_u = 0 \qquad (2,B.14)$$

Appropriate substitution into equation (2.B.11) yields

$$\ddot{\partial}_z = \frac{-k_1k_2k_3k_4 \quad \partial W}{1-[(s^{-2}k_2k_3k_4k_8)+(-s^{-1}k_3k_6k_7)]}$$

Reducing further, the transfer function is

$$\frac{\ddot{\partial Z}}{\partial W} = \frac{-k_1k_2k_3k_4 \quad s^2}{s^2+k_3k_6k_7s+k_2k_3k_4k_8} \qquad (2.B.15)$$

For the condition that control input is applied, the acceleration output has the following transform:

$$\ddot{\partial}_z = \frac{-k_3k_4k_7k_{10}s\,\partial_u}{s^2+k_3k_6k_7s+k_2k_3k_4k_8} - \frac{k_1k_2k_3k_4s^2 \quad \partial W}{s^2+k_3k_6k_7s+k_2k_3k_4k_8} \qquad (2,B.16)$$

Following the same procedure for the applied control input, the volumetric plenum air mass output has the following transfer function:

$$\Delta_3 = 1 - L_1 \qquad (2,B,17)$$

$$P_3 = k_{10}s^{-1} \qquad (2.B.18)$$

$$\Delta_2 = 1 \qquad (2.B.19)$$

$$P_4 = -k_1k_2k_3k_6 \qquad (2.B.20)$$

$$\partial V_m = \frac{k_{10}s+k_2k_3k_4k_8k_{10}s^{-1}}{s^2+k_3k_6k_7s+k_2k_3k_4k_8} \partial_u \qquad (2.B.21)$$

Equation (2.B.15) is of the form;

$$\frac{\text{OUTPUT}}{\text{INPUT}} = \frac{-as^2}{s^2+bs+c} \qquad (2.B.22)$$

and with no control action, becomes;

$$\frac{y(s)}{\partial W(s)} = \frac{as^2}{s^2+bs+c} \qquad (2.B.23)$$

where

$$y(s) = \partial\ddot{Z} \qquad (2,B.24)$$

and

$$\frac{\partial V_m(s)}{\partial W(s)} = \frac{b}{s^2+bs+c} \qquad (2.B,25)$$

where the coefficients consist of the following parameters;

$$a = -k_1 k_2 k_3 k_4 \qquad (2.B,26)$$

$$b = k_3 k_6 k_7 \qquad (2.B.27)$$

$$c = k_2 k_3 k_4 k_8 \qquad (2.B,28)$$

$$d = -k_1 k_2 k_3 k_6 \qquad (2.B,29)$$

The values of the coefficients, k_n, for the XR-3 craft are listed in Table I and were obtained from the results of the linearization process of Appendix A.

Special attention should be given to the coefficient that contains k_1 which is a sinc function of the form:

$$k_1 = \left[\left(\frac{2W_p V_w}{\omega_i}\right) \operatorname{Sin}\left(\frac{\omega_i L_p}{2V_w}\right)\right] \qquad (2.B.30)$$

k_1 may be simplified by an approximation detailed in Appendix A of Ref. 8. The simplification is based upon the fact that for ahead seas, the incident frequency. ω_i is;

$$\omega_i = \frac{1-\sqrt{1+4\left(\frac{V_s}{G}\right)\omega_e}}{-2\left(\frac{V_s}{G}\right)} \qquad (2,B.31)$$

For convenience in this study, the value of the ships velocity, V_s, is set equal to the gravitational constant, G. This value of V_s, when converted to knots, is 19.3 knots which is within

TABLE I

SYSTEM COEFFICIENT (k_n) VALUES

k_n	FORMULA	XR-3 VALUE
k_1	$\left(\frac{2W_P V_W}{\omega_i}\right)\sin\left(\frac{W_L L_P}{2V_W}\right)$	$2267.782 \dfrac{\sin\left(\frac{62.8319}{L_W}\right)}{\left(\frac{62.8319}{L_W}\right)}$
k_2	$\frac{1}{V_b(0)}$	3.5336×10^{-3}
k_3	$\gamma Pb(0)$	2996.0
k_4	$\frac{A_b}{M}$	1.0711
k_6	$nk_q + \frac{C_n A_l}{P_a}\sqrt{\frac{P_a}{2\overline{P_b}(0)}}$	6.14422
k_7	$\frac{1}{V_m(0)}$	3.5052×10^{-3}
k_8	A_b	200.0
k_{10}	CONSTANT	1.0

the operating range of the XR-3. Continuing;

$$\omega_i = \frac{1-\sqrt{1+4\omega_e}}{-2} \qquad (2.B.32)$$

It follows that

$$\omega_i^2 = \omega_e \qquad (2.B.33)$$

This approximation is valid for all $\omega_e > 2.5$ radians/sec. From the definition of the incident wave,

$$\omega_i^2 = \frac{2\pi g}{L_W} \qquad (2.B.34)$$

k_I becomes

$$k_1 = A_b \frac{\mathrm{Sin}(\frac{\omega_i L_P}{2V_\omega})}{(\frac{\omega_i L_P}{2V_\omega})} \qquad (2.B.35)$$

Where the horizontal area of the plenum chamber is

$$A_b = W_P L_P \quad . \qquad (2.B.36)$$

For a speed of 19.3 knots and since

$$L_W = \frac{2\pi g}{\omega_e} \qquad (2.B.37)$$

k_1 simplifies to;

$$k_1 = A_b \frac{\mathrm{Sin}(\frac{\pi L_p}{L_W})}{(\frac{\pi L_p}{L_W})} \qquad (2.B,38)$$

For the XR-3,

$$A_b = 200 \text{ ft}^2$$

$$L_p = 20 \text{ ft}$$

Then

$$a = k_1 = 2267,782 \frac{\mathrm{Sin}(\frac{62.8319}{L_W})}{(\frac{62.8319}{L_W})} \qquad (2.B,39)$$

From Equation (2.B,38), it can be seen that a null value for k_1 will occur for $nL_W = L_p$ and a peak value for k_1 will occur for $nL_W = L_p/2$ where n is an integer.

2. State Equation Development

The state equations are of the form

$$\dot{\underline{X}} = \underset{\sim}{A}\underline{X} + \underset{\sim}{B}\partial u + G\partial W \qquad (2.B.40)$$

where the state variable vector is chosen as

$$\underline{X} = (\partial_z, \dot{\partial}_z, \partial V_m)^T \qquad (2.B.41)$$

and the output variable

$$y = \ddot{\partial}_z = \underset{\sim}{C}\,\underline{X} + F\,\partial W \qquad (2,B.42)$$

The states are defined as

$$X1 = \partial Z = (Z - Z_{ss}), \text{ Incremental Heave(Draft)} \quad (2.B.43)$$

$$X2 = \partial \dot{Z} = (\dot{Z} - \dot{Z}_{ss}), \text{ Incremental Heave Rate} \quad (2.B.44)$$

$$X3 = \partial V_m = (V_m - V_{mss}), \text{ Incremental Air Mass Volume} \quad (2.B.45)$$

$$\text{where } V_m = \frac{M_b}{\rho_a} \quad (2.B.46)$$

with control defined as a scaler, rate of incremental change of air mass volume,

$$\partial_u = \partial \dot{V}_{m_c} \quad (2.B.47)$$

and where the sea input disturbance is ∂W.

From the signal flow graph of Fig. 2,

$$\partial V_m = (\partial_u k_{10} - k_6 \partial P_b) s^{-1} \quad (2.B.48)$$

$$X_1 = \partial_z = s^{-1} \partial \dot{z} \quad (2.B.49)$$

$$\dot{X}_1 = \partial \dot{z} = s^{-1} \partial \ddot{z} \quad (2.B.50)$$

$$\dot{X}_2 = \partial \ddot{z} = - \partial P_b k_4 \quad (2.B.51)$$

where

$$\partial P_b = (\partial V_m k_7 - k_2[-\partial W k_1 - k_8 \partial Z])k_3 \qquad (2.B,52)$$

Rearranging

$$\partial P_b = \partial V_m k_3 k_7 + k_1 k_2 k_3 \partial W + k_2 k_3 k_8 \partial Z \qquad (2.B,53)$$

and grouping in order of states

$$\partial P_b = k_2 k_3 k_8 \partial Z + k_3 k_7 \partial V_m + k_1 k_2 k_3 \partial W \qquad (2.B.54)$$

The output term, y is

$$y = \partial_z^{\cdot\cdot} \qquad (2.B.55)$$

Substituting equation (2,B,5) into equation (2.B.55) yields,

$$y = -k_2 k_3 k_4 k_8 \partial Z - k_3 k_4 k_7 \partial V_m - k_1 k_2 k_3 k_4 \partial W \qquad (2.B.56)$$

Finally, the incremental change in the volumetric air mass is written as

$$\dot{X}3 = \partial \dot{V}_m = (\partial u k_{10} - k_6 \partial P_b) \qquad (2,B,57)$$

$$= -k_2 k_3 k_6 k_8 \partial Z - k_3 k_6 k_7 \partial V_m$$

$$- k_1 k_2 k_3 k_6 \partial W + k_{10} \partial u \qquad (2,B.58)$$

Equations (2.B.50), (2.B.56) and (2.B.57) are the states of interest and are grouped below,

$$\dot{X}1 = X2 \tag{2.B.59}$$

$$\dot{X}2 = -k_2k_3k_4k_8X1 - k_3k_4k_7X3 - k_1k_2k_3k_4\,\partial W \tag{2.B.60}$$

$$\dot{X}3 = -k_2k_3k_6k_8X1 - k_3k_6k_7X3 - k_1k_2k_3k_6\,\partial W + k_{10}\,\partial u \tag{2.B.61}$$

with the output acceleration:

$$y = -k_2k_3k_4k_8X1 - k_2k_4k_7X3 - k_1k_2k_3k_4\,\partial W \tag{2.B.62}$$

Thus the linear system matrices are;

$$A = \begin{bmatrix} 0 & 1 & 0 \\ -k_2k_3k_4k_8 & 0 & -k_3k_4k_7 \\ -k_2k_3k_6k_8 & 0 & -k_3k_6k_7 \end{bmatrix} \tag{2.B.63}$$

$$B = \begin{bmatrix} 0 \\ 0 \\ 1 \end{bmatrix} \tag{2.B.64}$$

$$F = -k_1k_2k_3k_4 \tag{2.B.65}$$

$$G = \begin{bmatrix} 0 \\ -k_1k_2k_3k_4 \\ -k_1k_2k_3k_6 \end{bmatrix} \tag{2.B.66}$$

Computer simulation of the linear system was accomplished using the Naval Postgraduate School program "IODE" operated from the CPCMS terminal of the IBM-360. See Appendix C for IODE listing. The program ocean generator for ∂W inputs a single frequency at a time using the special function feature. Wavelength (L_W) will change with encounter frequency (ω_e) as shown in equation (2.B,35). It should be remembered that the craft speed is constant at 19,3 knots for the data base of this design.

3. The Characteristic Equation

The characteristic equation under no control conditions of operation, is formed from the $\underset{\sim}{A}$ matrix (see Appendix A),

$$\text{DET}(SI-A) \tag{2.B.67}$$

$$\text{DET}\begin{vmatrix} s & -1 & 0 \\ 2267.782 & s & 11.248 \\ 13002.8 & 0 & 64.493s \end{vmatrix} \tag{2.B.68}$$

Then the characteristic equation is;

$$s^3+64.493s^2+2267.782s+.5701 \tag{2.B.69}$$

which factors into

$$(s+2.5414x10^{-4})(s+32.25+J35.04)(s+32.25-j35.04) \tag{2.B.70}$$

and is shown in the pole-zero map of Fig. 3. Note that the dominant pole is a real pole close to the origin. Also note that the complex pair will affect early time response since they are relatively far removed from the origin.

A root locus plot with no control input is shown in Fig. 4. The plot covers a range of

$$5 < k_6 < 26 \tag{2.B.71}$$

Table II lists the characteristic equation roots for the range

$$5 < k_6 < 50 \tag{2.B.72}$$

As can be seen from equation (2.B.63), k_6 is present in both the a_{31} and a_{33} system coefficients. In order to perform the root locus study, the characteristic equation was rearranged to show the adjustable parameter k_6;

$$s^3+k_3k_7s^2+k_2k_3k_4k_8s+k_6(k_3k_4k_7k_2k_3k_8+k_2k_3k_4k_8k_3k_7)+k_6s^2 \tag{2.B.73a}$$

with parameter values

$$s^3+(k_6+10.5016)s^2+2267.782s+.0928k_6 \tag{2.B.73b}$$

From the table and root locus plot, it can be seen that as k_6 becomes large, the complex root pair become real with one

root moving toward the origin and the other migrating to negative infinity. Additionally, the pole near the origin moves very little and remains real throughout the excursion of k_6. It was observed that this was very similar to the root locus plot in the air flow study conducted in Ref. 1. However, the removal of the buoyancy term in this study caused the pole near the origin to stay real whereas the same pole in Ref. 1 became immaginary for large values of k_6. The root locus demonstrated the high sensitivity of the complex pair to changes in air flow rate, while the pole near the origin exhibited a very low sensitivity to changes in k_6. This observation further demonstrated that the vertical oscillatory characteristics of the ship depend upon changes in k_6.

As a further check on the effect of air flow on C.G. acceleration, an investigation of the effect of changing k_6 on the frequency spectrum of C.G. accleration was conducted and the results are shown in Appendix D. From these results it seemed appropriate to seek a control law that would adjust k_6, the air flow rate, In an effort to gain a better understanding of the effect of various air flow rates on the system, a sensitivity and stability analysis was performed in section IVB. The ROOTLO program used in the above study is shown in Appendix C.

Figure 3

POLE/ZERO PLOT FOR THE CHARACTERISTIC EQUATION WITH NOMINAL AIR FLOW RATE $s^3+64.493s^2+2267.782s+.5701$

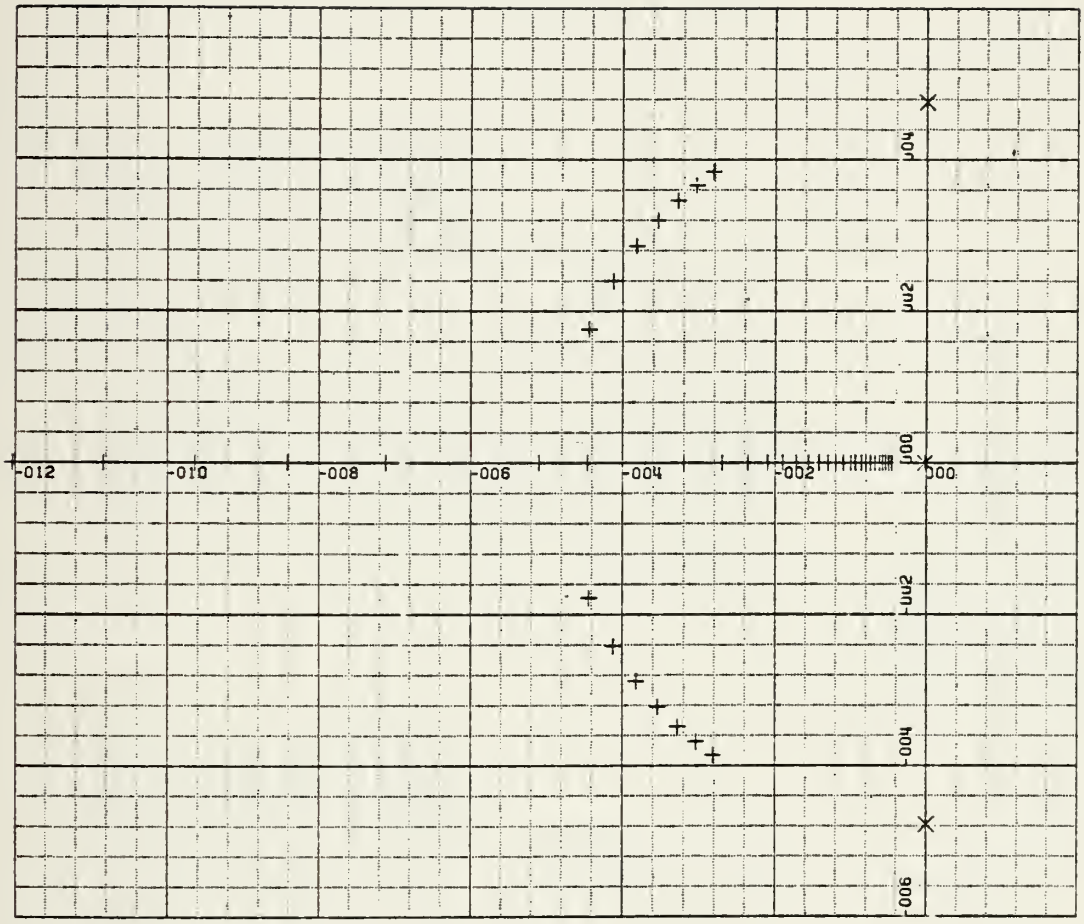

X-SCALE=2.00E+01 UNITS INCH.
Y-SCALE=2.00E+01 UNITS INCH.
ROOT LOCUS PLOT FOR MODIFIED
PRESSURE ONLY LINEAR MODEL

Figure 4

k_6	α	β	γ
5.000	$1.256\times10^{-4}+J\,4.762\times10^{1}$	$1.256\times10^{-4}-J\,4.762\times10^{1}$	-2.513×10^{-4}
5.393	$-2.809\times10^{1}+J\,3.845\times10^{1}$	$-2.809\times10^{1}-J\,3.45\times10^{1}$	-2.513×10^{-4}
5.817	$-3.030\times10^{1}+J\,3.673\times10^{1}$	$-3.030\times10^{1}-J\,3.673\times10^{1}$	-2.513×10^{-4}
6.274	$-3.268\times10+J\,3.463\times10^{1}$	$-3.267\times10^{1}-J\,3.463\times10^{1}$	-2.513×10^{-4}
6.768	$-3.525\times10^{1}+J\,3.201\times10^{1}$	$-3.525\times10^{1}-J\,3.201\times10^{1}$	-2.513×10^{-4}
7.300	$-3.802\times10^{1}+J\,2.866\times10^{1}$	$-3.802\times10^{1}-J\,2.866\times10^{1}$	-2.513×10^{-4}
7.875	$-4.102\times10^{1}+J\,2.418\times10^{1}$	$-4.102\times10^{1}-J\,2.418\times10^{1}$	-2.513×10^{-4}
8.494	$-4.424\times10^{1}+J\,1.760\times10^{1}$	$-4.424\times10^{1}-J\,1.760\times10^{1}$	-2.513×10^{-4}
9.162	$-5.089\times10^{1}+J\,0.0$	$-4.455\times10^{1}-J\,0.0$	-2.513×10^{-4}
9.883	$-7.103\times10^{1}+J\,0.0$	$-3.192\times10^{1}-J\,0.0$	-2.513×10^{-4}
1.066	$-8.409\times10^{1}+J\,0.0$	$-2.696\times10^{1}-J\,0.0$	-2.513×10^{-4}
11.49	$-9.622\times10^{1}+J\,0.0$	$-2.356\times10^{1}-J\,0.0$	-2.513×10^{-4}
12.40	$-1.082\times10^{2}+J\,0.0$	$-2.094\times10^{1}-J\,0.0$	-2.513×10^{-4}
13.37	$-1.205\times10^{2}+j\,0.0$	$-1.880\times10^{1}-J\,0.0$	-2.513×10^{-4}

TABLE II

ROOTS FOR MODIFIED PRESSURE LIFT

ONLY MODEL, NO CONTROLS

III. VERIFICATION OF THE MODEL

A. LINEAR AND NONLINEAR SYSTEM VALIDATION

The validation of the simplified model of a single variable pressure lift force was conducted by comparison of its frequency response characteristics with those of the model presented in Ref. 1. Several techniques were used to accomplish this.

1. Single frequency constant amplitude sinusoids were applied to both the nonlinear system of Fig. 1 and also the linear system of Fig. 2. The acceleration output signal for the nonlinear system is shown in Fig. 5. Its sinusoidal form, in steady state indicates the linearity of the system, which was the case throughout the frequency range.
2. The linear transfer function of center of gravity acceleration (Eq. 2.B.15) was subjected to a constant wave height input using a spectrum of discrete encounter frequencies. The heave accelerations were converted to dB and plotted in a bode diagram shown in Fig. 6
3. Discrete fourier transform technique, developed in an independent study by S. Carpenter, [Ref. 9], was also used to test the response of the linear system (Fig. 9) to an irregular sea input shown in Fig. 7

consisting of twelve components of frequency and amplitude from the Pierson-Moskowitz energy density spectrum given in Fig. 8 [Ref. 8, 9].

The results of procedures 2 and 3 above were compared with the linear system response of Ref. 1. The magnitudes for the center of gravity acceleration showed approximately 20% difference between the pressure lift only, no control, response curve (Fig. 6) and the linear system of Ref. 1 (Fig. 10). The general shape of the curves are identical. Therefore, the pressure lift only model was assumed to be valid and useful for linear regulator control design. The observed peaks and nulls of Figs. 6, 10 are a result of the sinc function numerator coefficient, k_1, as described in Section III. The relationship between plenum length (L_p) and wavelength (L_w) expressed in k_1, determine where, in the encounter frequency spectrum, the nulls and peaks occur.

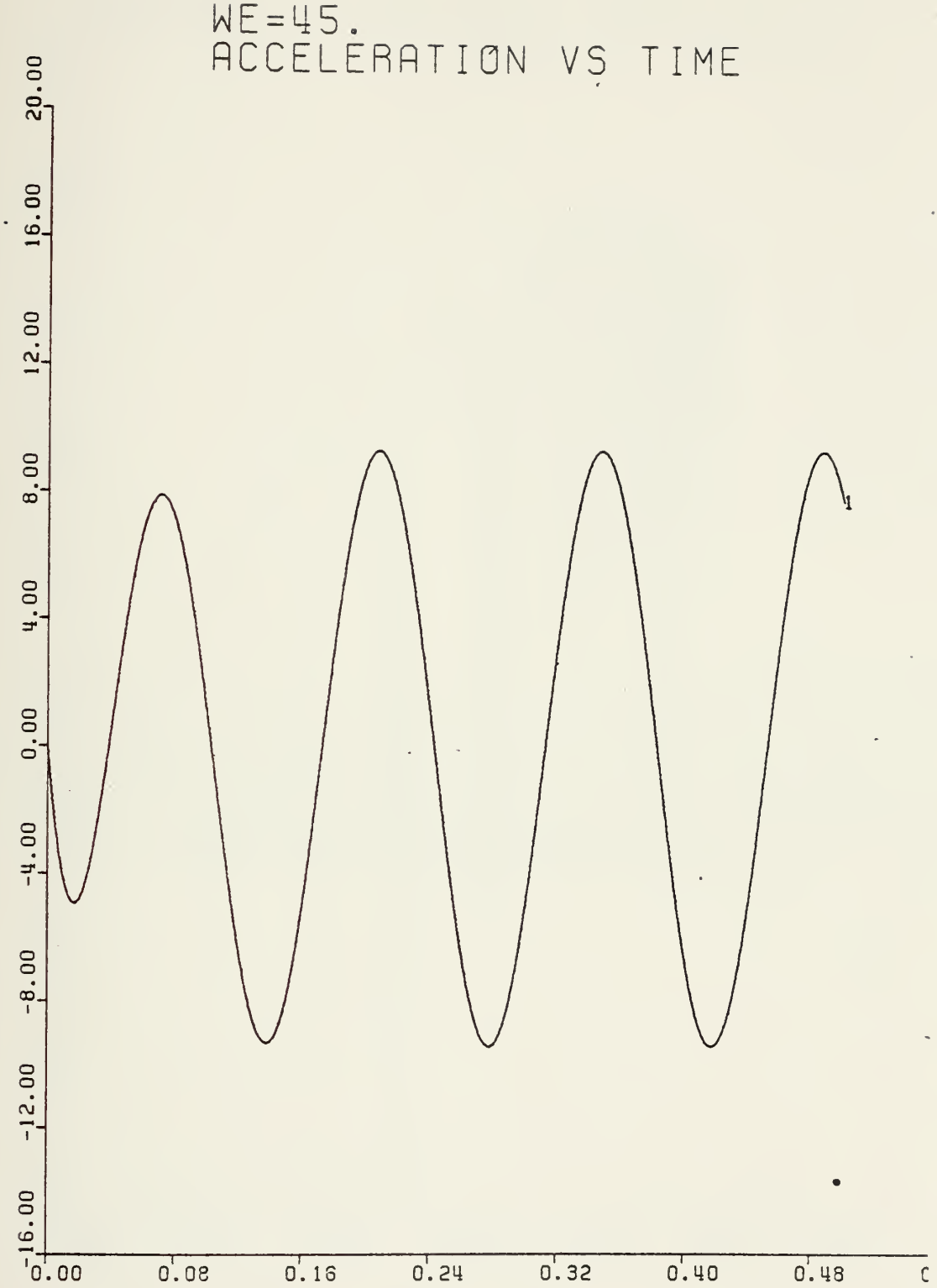

XSCALE= 0.08 UNITS/INCH
YSCALE= 4.00 UNITS/INCH

Figure 5

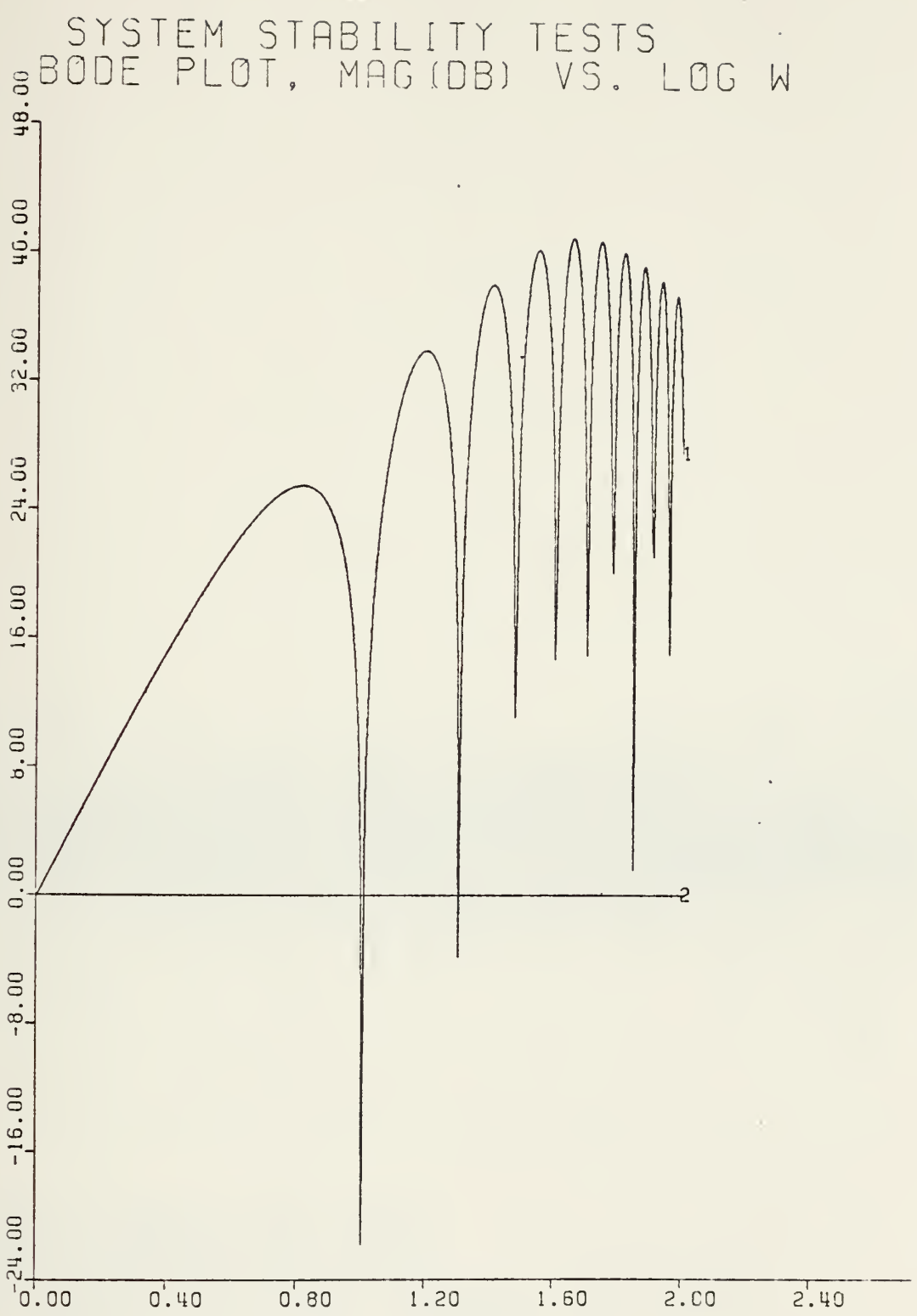

XSCALE= 0.40 UNITS/INCH
YSCALE= 8.00 UNITS/INCH

Figure 6

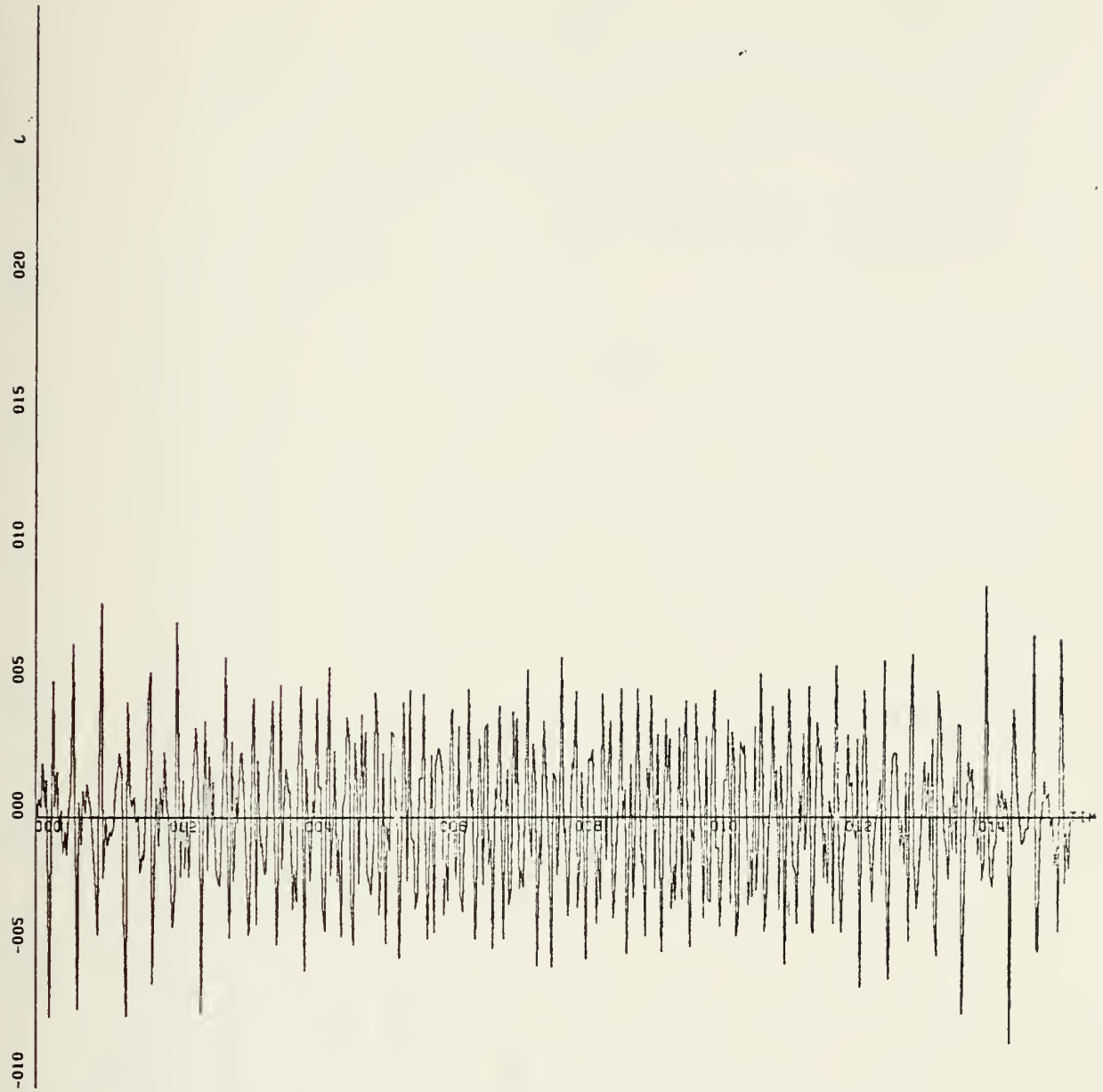

X-SCALE=2.00E+00 UNITS INCH.
Y-SCALE=5.00E+00 UNITS INCH.
TIME HISTORY OF SES(2) RESPONSE
TO IRREGULAR SEA RUN1

Figure 7

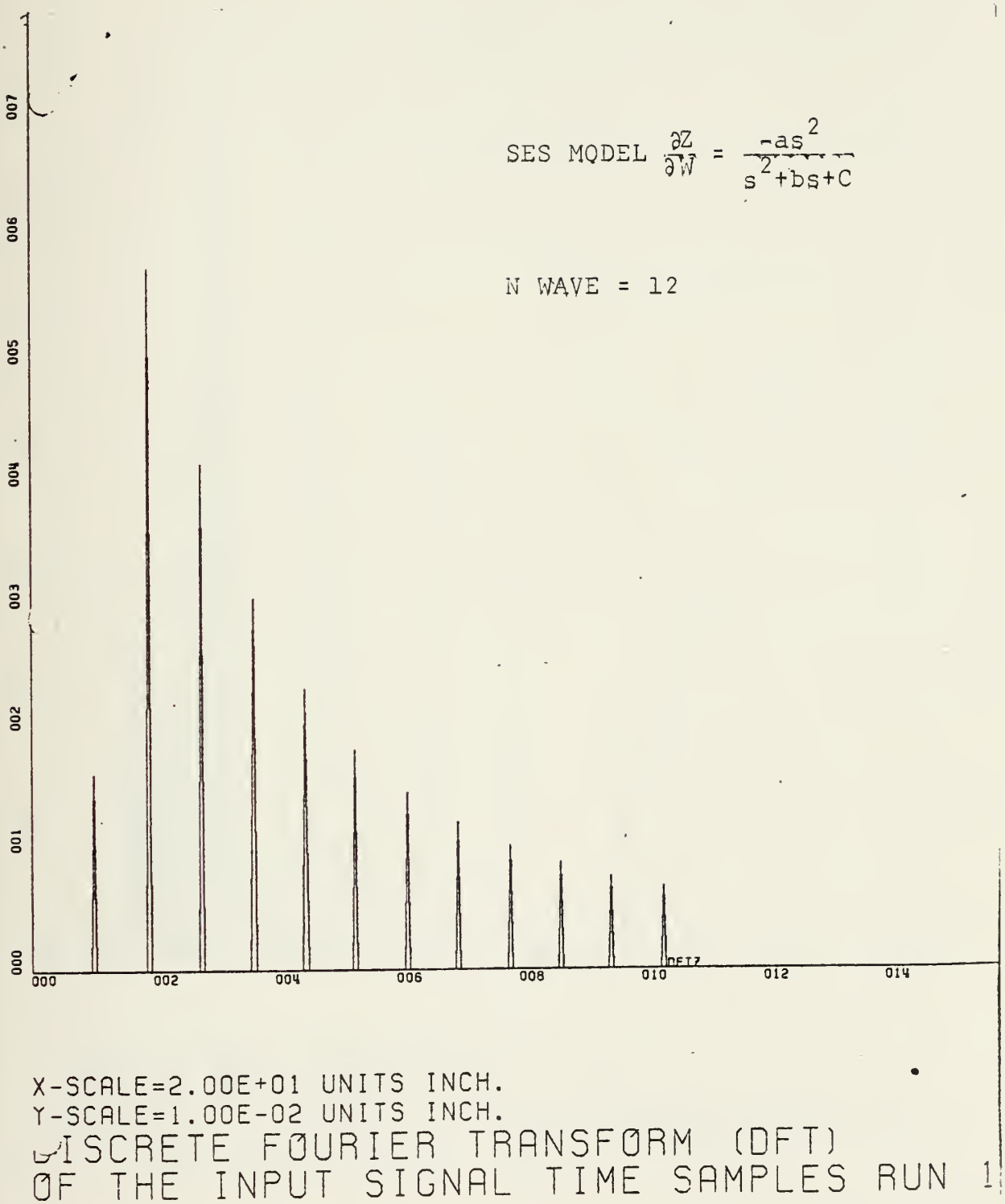
SES MODEL $\frac{\partial Z}{\partial W} = \frac{-as^2}{s^2+bs+C}$
N WAVE = 12
007
006
005
004
003
002
001
000
000
002
004
006
008
010
012
014
DFTZ
X-SCALE=2.00E+01 UNITS INCH.
Y-SCALE=1.00E-02 UNITS INCH.
DISCRETE FOURIER TRANSFORM (DFT)
OF THE INPUT SIGNAL TIME SAMPLES RUN 1

Figure 8

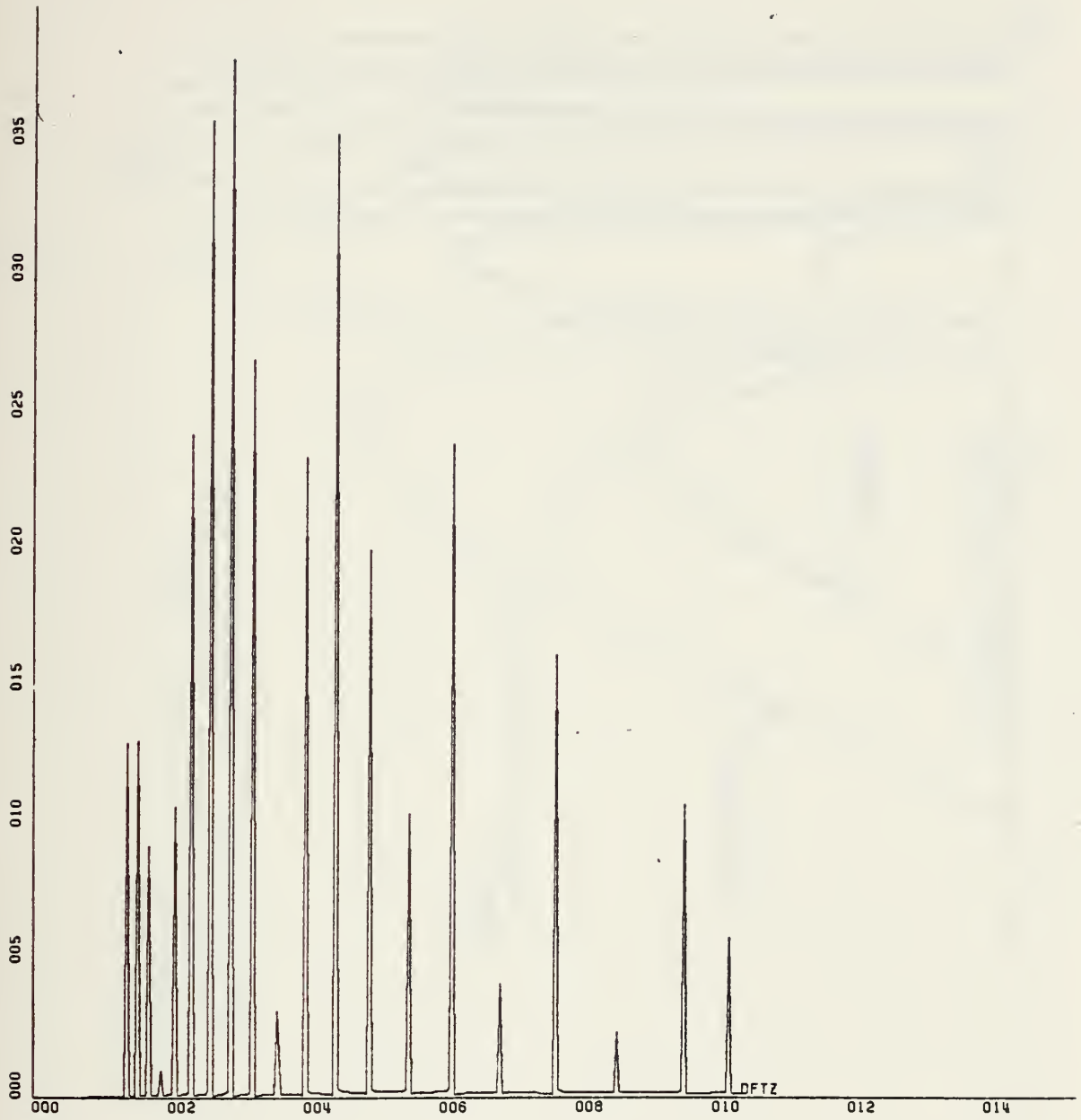

X-SCALE=2.00E+01 UNITS INCH.
Y SCALE=5.00E-01 UNITS INCH.
DISCRETE FOURIER TRANSFORM OF SES(2)
TO IRREGULAR SEA RUN1

Figure 9

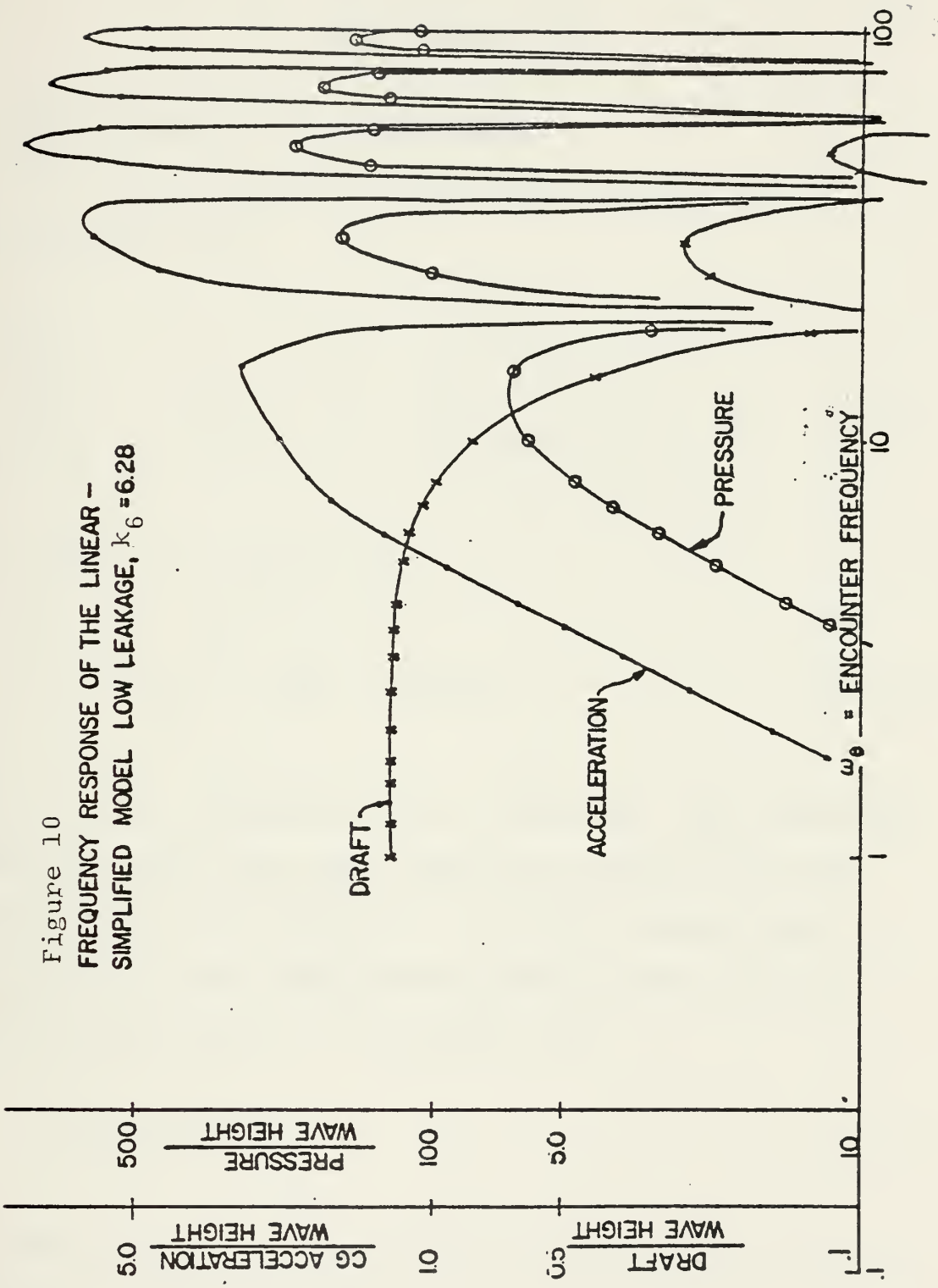

Figure 10
FREQUENCY RESPONSE OF THE LINEAR - SIMPLIFIED MODEL LOW LEAKAGE, K_6 =6.28

IV. THE CONTROL LAW

A. LINEAR REGULATOR DESIGN APPROACH

The linear pressure lift only model is described in state equation form;

$$\begin{bmatrix} \dot{X}_1 \\ \dot{X}_2 \\ \dot{X}_3 \end{bmatrix} = \begin{bmatrix} 0 & 1 & 0 \\ a_{21} & 0 & a_{23} \\ a_{31} & 0 & a_{33} \end{bmatrix} \begin{bmatrix} X_1 \\ X_2 \\ X_3 \end{bmatrix} + \begin{bmatrix} 0 \\ 0 \\ 1 \end{bmatrix} \partial_u \qquad (4.A.1)$$

with the cost function of the form

$$J = 1/2 \int_0^T (\underline{X}^T \underset{\sim}{Q} \underline{X} + \partial \underline{U}^T \underset{\sim}{R} \partial \underline{U}) \qquad (4.A.2)$$

where the final value error is not included. The system may be designed using the linear regulator technique with the given quadratic cost function. An optimal control was found using both the transient and steady state solutions of the Riccati equation. The control law

$$\partial \underline{U}^* = -\underset{\sim}{R}^{-1} \underset{\sim}{B}^T \underset{\sim}{K} \underline{X} \qquad (4.A.3)$$

where the $\underset{\sim}{K}$ matrix was found from the solution of the Riccati equation

$$\dot{K} = -\underline{KA} - A^T\underset{\sim}{K} - \underset{\sim}{Q} + \underset{\sim}{K}\,\underset{\sim}{B}\,\underset{\sim}{R}^{-1}B^T\underset{\sim}{K} \qquad (4.A.4)$$

with the appropriate choice of the $\underset{\sim}{Q}$ and $\underset{\sim}{R}$ coefficients, the feedback gains for the system were calculated. Unfortunately, the first choice for $\underset{\sim}{Q}$ and $\underset{\sim}{R}$ may not yield control gains which are physically realizable or practical. For this reason, it is appropriate to examine the effects of the control gains on the pole location in the s plane for the controlled system. Such a study was done and is presented in part B of this section. The choices for $\underset{\sim}{Q}$ and $\underset{\sim}{R}$ were derived by trial and error. However, the design criterion was to reduce this magnitude of the frequency response curves through the study of various Bode plots. To this end, many $\underset{\sim}{Q}$ and $\underset{\sim}{R}$ values were tried.

The Riccati equation computations were done using a computer program documented in Ref. 10 and modified by B. DesJardins in Ref. 11. Appendix C illustrates the input/output format of this program. Based upon the above design criterion, the final weighting matrix chosen was;

$$Q = \begin{bmatrix} 10^5 & 0 & 0 \\ 0 & 10^3 & 0 \\ 0 & 0 & .5 \end{bmatrix} \qquad (4.A,5)$$

and

$$R = .03$$

The optimal control gains obtained using the above $\underset{\sim}{Q}$ and $\underset{\sim}{R}$ matrixes were;

$$g_{11} = -1.689 \times 10^{3}$$
$$g_{12} = 1.19 \times 10^{2} \qquad (4.A.6)$$
$$g_{13} = -1.83 \times 10^{1}$$

These gains were multiplied by their respective states and applied to the state equations (2.B.59, 61, 62). Under state feedback control, the resultant output acceleration frequency magnitude was reduced by 13% from the peak no control magnitude. Table III lists the peak lobe values of the C.G. Acceleration/wave height magnitudes versus frequency for the nonlinear and linear systems. Each system was exercised under control and no control conditions. The steady state sinusoidal output for the linear model, under control and no control conditions is shown in Table IV for ω_e=45 rad/sec, where

$$\partial_u = g_{11}X1 + g_{12}X_2 + g_{13}X_3 \qquad (4.A.7)$$

and

$$y = \ddot{\partial Z} \qquad (4.A.8)$$

The control signal for the nonlinear system was generated by using the linear control low coefficient found using linear regulator theory. The reduction in acceleration was not uniform throughout the frequency range. At law frequencies, ω_e<17 rad/sec, control gains caused an increase in C.G. acceleration.

As ω_e approached 100 rad/sec, C.G. acceleration approached but never exceeded the no control condition. Effective control was realized in the frequency range $17<W_e<100$ radians/sec.

B. SENSITIVITY AND STABILITY

Since a set of optimal gains were found for the system, it remained to test the system under feedback control and observe the sensitivity and stability for acceptability.

The locus of roots of the characteristic equation for the pressure lift only system without state feedback control was shown in Section III. The objective of state feedback control is to adjust the position of the complex pair of roots in such a way as to reduce center of gravity accelerations. For the open control loop, the transfer function was shown (Eq. 2.B.22) to be

$$\frac{\partial \ddot{Z}}{\partial W} = \frac{-as^2}{s^2+bs+c} \qquad (4.B.1)$$

Addition of state feedback will change the value of b and c. Note that if the k_1 sinc function null effects are removed from the numerator, then a=c. It follows that the magnitude of the Bode plot will reach unity value at high frequency regardless of changes in b and c. In other words, the system has high pass frequency characteristics. Thus, the results of increasing the value of c will be a reduction of the magnitude plot in the lower range of frequencies of interest. Also, note that changes in the b coefficient will affect the resonant peaking at the corner frequency.

TABLE III

PEAK LOBE VALUES OF FREQUENCY RESPONSE, PRESSURE LIST ONLY LINEAR & NONLINEAR MODELS UNDER CONTROL AND NO CONTROL CONDITIONS

ω_e	NONLINEAR		LINEAR	
	NO CONTROL	CONTROL	NO CONTROL	CONTROL
6	18.6	26.5	18.5	27.8
7	18.5	25.2	18.6	26.6
8	15.7	20.3	15.7	21.4
9	9.7	12.7	9.8	12.7
14	42.2	42.2	42.3	45.7
15	48.2	48.2	48.4	50.9
16	49.7	49.7	49.9	51.1
17	45.9	45.9	46.1	46.2
24	69.8	62.9	70.5	63.4
25	78.1	69.7	79.0	70.3
26	79.1	70.0	79.9	70.6
27	72.1	63.4	72.8	63.9
28				
34	90.8	77.7	91.8	78.5
35	100.8	86.3	101.8	87.3
36	102.4	86.8	102.3	87.9
37	91.7	78.6	92.6	79.6
38				
44	99.5	86.8	100.1	87.4
45	110.0	96.4	113.0	98.6
46	110.0	96.8	111.5	98.0
47	99.7	88.0	101.0	88.9
48				
54	97.1	88.5	97.5	88.5
55	107.7	98.5	108.0	98.7
56	108.1	99.2	108.8	100.0
57	98.2	90.5	99.0	91.2

TABLE III
(continued)

ω_e	NONLINEAR		LINEAR	
	NO CONTROL	CONTROL	NO CONTROL	CONTROL
64	88.7	83.8	89.3	84.3
65	99.3	94.1	99.5	94.8
66	100.4	95.4	101.1	96.5
67	91.9	87.6	91.9	88.0
68				
69				
74	79.0	76.5	79.4	77.0
75	89.5	86.9	89.9	87.3
76	91.3	88.8	91.3	88.6
77	84.4	82.2	84.8	82.6
78				
79				
84	69.9	68.8	70.1	69.0
85	80.2	78.9	80.1	79.3
86	82.6	81.4	83.0	81.7
87	77.4	76.1	77.0	76.5
94	61.9	61.4	62.0	61.5
95	71.9	71.5	72.1	71.6
96	75.0	74.5	75.2	74.7
97	70.9	70.5	70.9	70.6

TABLE IV

SINUSOIDAL LINEAR MODEL OUTPUT WITH/WITHOUT FEEDBACK CONTROL AT ω_e=45.0 Rad/Sec.

TIME T	CONTROL Y	CONTROL EFFORT ∂_u	NO CONTROL Y
0.780	54.38	4.28	61.02
0.785	34.33	2.64	38.03
0.790	12.50	0.86	13.08
0.795	-9.96	-0.95	-12.54
0.800	-31.91	-2.72	-37.52
0.805	-52.23	-4.35	-60.56
0.810	-69.85	-5.76	-80.49
0.815	-83.86	-6.87	-96.26
0.820	-93.56	-7.62	-107.08
0.825	-98.44	-7.99	-112.38
0.830	-98.23	-7.94	-111.88
0.835	-92.97	-7.48	-105.62
0.840	-82.90	-6.64	-93.92
0.845	-68.60	-5.45	-77.37
0.850	-50.74	-3.97	-56.85
0.855	-30.27	-2.32	-33.39
0.860	-8.34	-0.53	-8.21
0.865	14.22	1.29	17.40
0.870	35.95	3.04	42.10
0.875	55.82	4.63	64.64
0.880	72.82	5.99	83.85
0.885	86.06	7.03	98.73
0.890	94.87	7.72	108.53
0.895	98.79	8.00	112.73
0.900	97.61	7.88	111.11
0.905	91.42	7.34	103.79
0.910	80.50	6.43	91.11
0.915	65.44	5.19	73.74
0.920	47.01	3.68	52.56
0.925	26.49	1.98	28.68
0.930	3.94	0.17	3.31

1. The Characteristic Equation For Feedback Control Applied

The signal flow graph of Fig. 2 was modified to show feedback gains and is shown in Fig. 11. Using Masons gain rule, the characteristic equation was derived from the S.F.G. (Eq. 4.B.10). The resulting equation was compared to characteristic equation derived from the modified system matrix with feedback of Appendix D. It was noted that they differ by the terms

$$a_{21}a_{33} \text{ and } -a_{23}a_{31} .$$

These terms very nearly cancel and are insignificant ($a_{21}a_{33}-a_{23}a_{31}=.5701$) when compared with the other larger terms in the characteristic equation. Therefore, their omission from the signal flow graph of Fig. 11 is valid. The derivation follows:

$$L_1 = \frac{-g_3}{s} = \frac{-g_3}{s} = \frac{-g_3}{s} \qquad (4.B.2)$$

$$L_2 = \frac{(k_3)(-k_6)(-k_7)}{s} = \frac{-k_3k_6k_7}{s} = \frac{-a_{33}}{s} \qquad (4.B.3)$$

$$L_3 = \frac{(-k_2)(k_3)(-k_4)(-k_8)}{s^2} = \frac{-k_2k_3k_4k_8}{s^2} = \frac{-a_{21}}{s^2} \qquad (4.B.4)$$

$$L_4 = \frac{(k_7)(k_3)(-k_4)(g_2)}{s^2} = \frac{-k_3k_4k_7}{s^2}g_2 = \frac{a_{23}}{s^2}g_2 \qquad (4.B.5)$$

$$L_5 = \frac{(k_7)(k_3)(-k_4)(-g_1)}{s^3} = \frac{k_3k_4k_7}{s^3}g_1 = \frac{a_{23}}{s^3}g_1 \qquad (4.B.6)$$

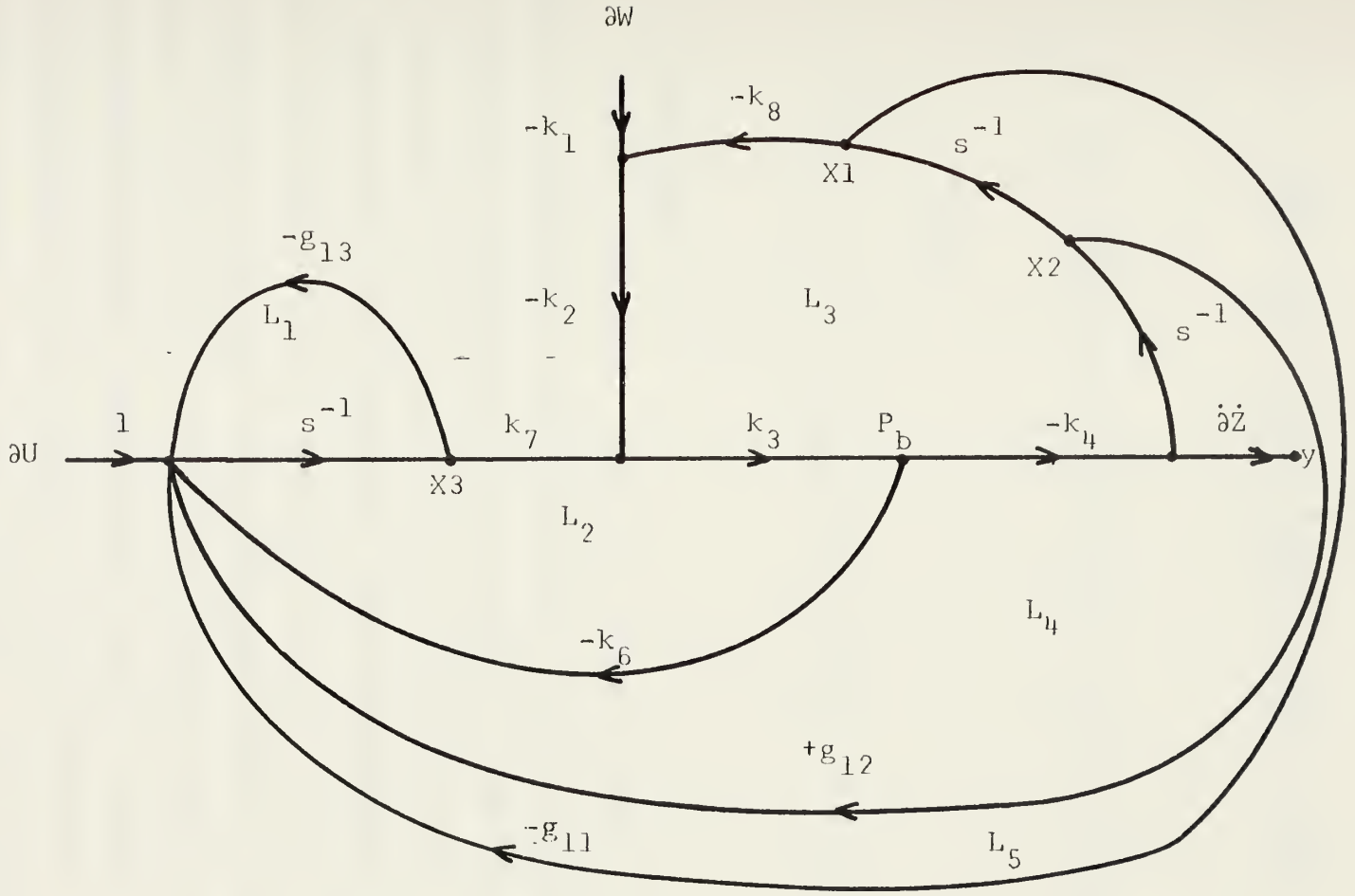

Figure 11

Linear Pressure Lift Only
Signal Flow Graph With State Feedback Control

$$\Delta = 1-[L_1+L_2+L_3\ L_4+L_5] + L_1\ L_3 \qquad (4.B.7)$$

$$\Delta = 1-[\frac{g_3}{s} - \frac{a_{33}}{s} - \frac{a_{21}}{s^2} - \frac{a_{23}}{s^2}\ g_2 + \frac{a_{23}}{s^3}\ g_1]+(\frac{g_3}{s})(\frac{-a_{21}}{s^2}) \qquad (4.B.8)$$

$$\Delta = \frac{1}{s^3}\ (s^3+g_3s^2 + a_{33}s^2 + a_{21}s + a_{23}g_2s - a_{23}g_1 + a_{21}g_3) \qquad (4.B.9)$$

$$s^3+(a_{33}+g_3)s^2 + (a_{23}g_2+a_{21})s + (a_{21}g_3 - a_{23}g_1) \qquad (4.B.10)$$

2. Root Locus

The following root locus plots are a study of the effects of changing the three different control feedback gains. Many weighting combinations were tried and it was discovered that the system was most sensitive to changes in air flow rates. This observation was in agreement with the analysis of Section II that the system was most sensitive to k_6. Each of the following root locus plots and associated table of values was chosen as representative of the alternatives tried. The characteristic equation used is shown as Eq. (4.B.10). The Naval Postgraduate School program for the IBM 360/67 computer was used to generate the tables and plots. The program listing is shown in Appendix C.

In the first study, the constant gains used were

$$g_{11} = 425.0 \ , \ g_{12} = 91$$

and g_{13} was varied over three decades starting from $g_{13} = .1$. The resultant plot and table of values are shown in Fig. 12 and Table IV respectively. For ease of reference, the system poles were given letter designations for the characteristic equation

$$(S+A)(S+B)(S+C) = 0 \qquad (4.B.11)$$

where

$$A = (+32.25-j35.04)$$

$$B = (+32.25+j35.04)$$

$$C = (2.5x10^{-4}+j0)$$

As g_{13} nears -20, pole a rapidly enters the real axis and migrates towards negative infinity and pole B moves upward across the real axis. Pole C moves in a negative direction until g_{13}=-26 and then moves below the real axis tracking the mirror image path of pole B. It was seen from this plot that as g_{13} nears -20 that the complex pair undergoes the greatest movement. In this study there was no point at which instability occurred. When the gains were tested on the system, there was no noticable decrease in vertical acceleration.

The next phase of this investigation uses constant gains of

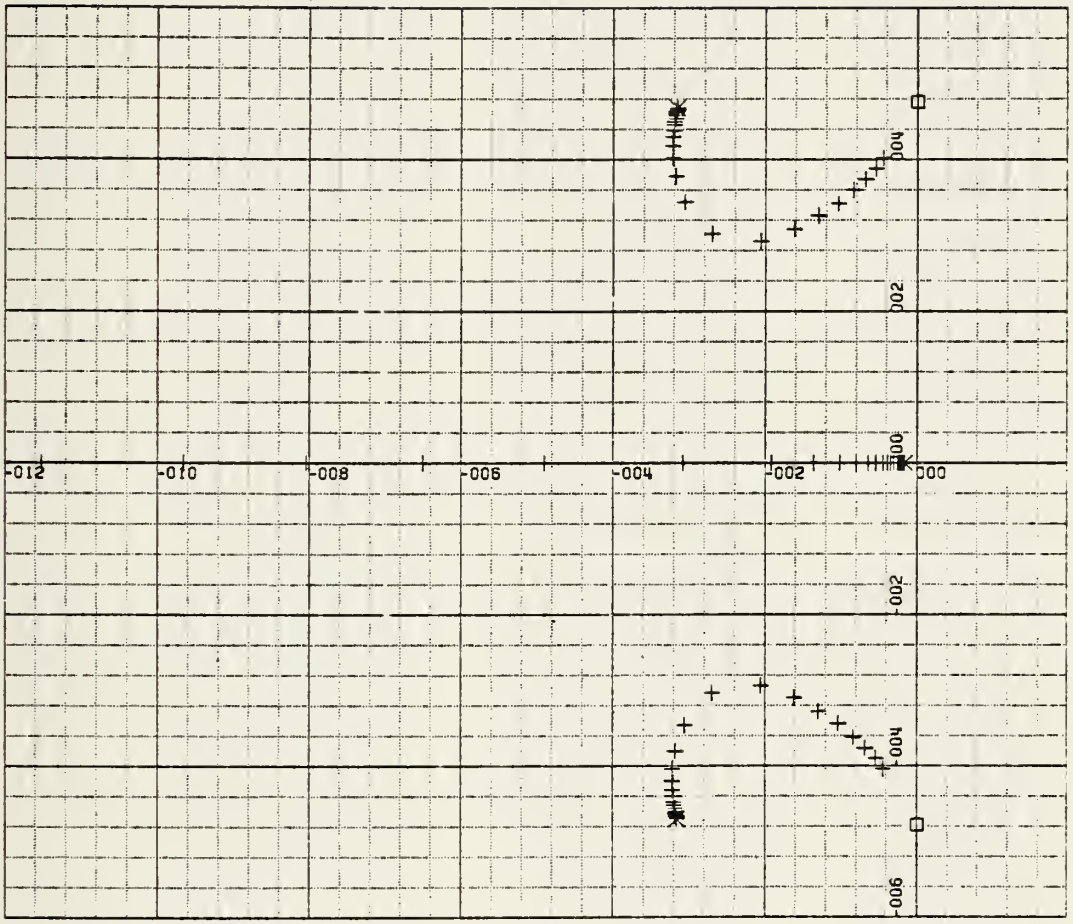

X-SCALE=2.00E+01 UNITS INCH.
Y-SCALE=2.00E+01 UNITS INCH.
ROOT LOCUS PLOT FOR MODIFIED
PRESSURE ONLY LINEAR MODEL

Figure 12

TABLE IV

Roots For Modified Pressure Lift Only Model, g_{11}=425.0, g_{12}=91, g_{13} Varies

k_6	A	B	C
-0.099	-31.49+j46.96	-31.49-j46.96	-1.49+j0
-0.127	-31.52+j46.88	-31.52-j46.88	-1.586+j0
-0.162	-31.52+j46.86	-31.52-j46.86	-1.611+j0
-0.207	-31.53+j46.84	-31.53-j46.84	-1.643+j0
-0.263	-31.53+j46.81	-31.53-j46.81	-1.684+j0
-0.335	-31.54+j46.76	-31.54-j46.76	-1.736+j0
-0.427	-31.55+j46.71	-31.55-j46.71	-1.802+j0
-0.544	-31.57+j46.64	-31.57-j46.64	-1.887+j0
-0.693	-31.59+j46.56	-31.59-j46.56	-1.995+j0
-0.883	-31.61+j46.45	-31.61-j46.45	-2.134+j0
-1.125	-31.64+j46.30	-31.64-j46.30	-2.312+j0
-1.433	-31.68+j46.12	-31.68-j46.12	-2.540+j0
-1.825	-31.72_j45.88	-31.72-j45.88	-2.835+j0
-2.326	-31.77+j45.58	-31.77-j45.58	-3.216+j0
-2.962	-31.84+j45.18	-31.84-j45.18	-3.711+j0
-3.773	-31.91_j44.67	-31.91-j44.67	-4.359+j0
-4.807	-31.99+j43.99	-31.99-j43.99	-5.214+j0
-6.124	-32.06+j43.08	-32.06-j43.08	-6.359+j0
-7.801	-32.09+j41.87	-32.09-j41.87	-7.923+j0
-9.937	-32.03+j40.20	-32.03-j40.20	-10.134+j0
-12.658	-31.70+j37.87	-31.70-j37.87	-13.450+j0
-16.125	-30.60+j34.50	-30.60-j34.50	-19.032+j0
-20.540	-26.95+j30.22	-26.95-j30.22	-30.645+j0
-26.165	-48.97+j0	-20.53+j29.31	-20.534-j29.31
-33.331	-64.98+j0	-16.02+j30.86	-16.023-j30.86
-42.458	-80.26+j0	-12.84+j32.65	-12.838-j32.65
-54.085	-96.55+j0	-10.36+j34.38	-10.367-j34.38
-68.90	-115.02+j0	-8.36+36.02	-8.363-j36.02

$$g_{11} = -195.32, \quad g_{12} = 34.98$$

while g_{13} varied over two decades from -.1. These gains were calculated from the Riccati with weighting matrix;

$$\underset{\sim}{Q} = \begin{bmatrix} 10^4 & 0 & 0 \\ 0 & 12^2 & 0 \\ 0 & 0 & .5 \end{bmatrix} \qquad (4.B.12)$$

and

$$R = .03 \qquad (4.B.13)$$

The resulting plot and table of pole values are shown in Fig. 13 and Table V respectively. As g_{13} varies, the poles follow similar paths as in the previous study. The greatest degree of pole movement, or sensitivity, occurs at g_{13}=-16.0. This set of gains produced instability when g_{13}>-1.08.

In the final study, the constant gains were

$$g_{11} = -1688.095, \; g_{12} = 119.16, \; g_{13} = -18.306$$

Again, g_{13} was made to vary over three decades starting with $g_{13} = -.1$. The resultant plot and table of values are shown in Fig. 14 and Table VI respectively. These gains were calculated using the $\underset{\sim}{Q}$ and $\underset{\sim}{R}$ values shown in (4,A.5). Again, the poles follow similar paths but pass closer to the origin than in the previous two studies, causing a greater net decrease in the systems oscillatory tendencies. As in the

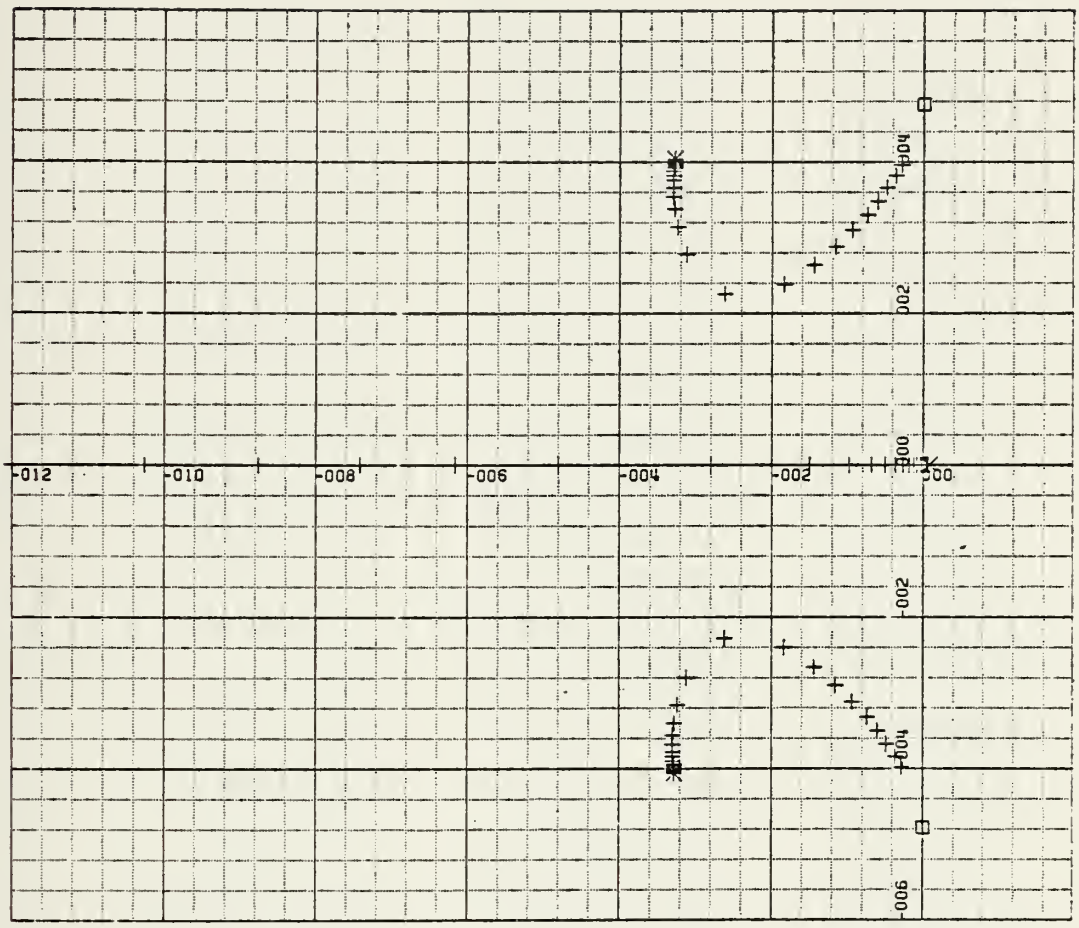

X-SCALE=2.00E+01 UNITS INCH.
Y-SCALE=2.00E+01 UNITS INCH.
ROOT LOCUS PLOT FOR MODIFIED
PRESSURE ONLY LINEAR MODEL

Figure 13

TABLE V

Roots For Modified Pressure Lift Only Model, g_{11}=-195.32, g_{12}=34.98, g_{13}=varies

k_6	A	B	C
-0.099	-32.65+j40.60	-32.56-j40.60	0.81+j0
-0.127	-32.66+j40.50	-32.66-j40.50	0.71+j0
-0.162	-32.67+j40.48	-32.67-j40.48	0.68+j0
-0.207	-32.67+j40.45	-32.69-j40.45	0.64+j0
-0.263	-32.67+j40.41	-32.67-j40.41	0.60+j0
-0.335	-32.68+j40.35	-32.68-j40.35	0.54+j0
-0.427	-32.69+j40.29	-32.69-j40.29	0.46+j0
-0.544	-32.70+j40.20	-32.70-j40.20	0.37+j0
-0.693	-32.71+j40.09	-32.71-j40.10	0.25+j0
-0.883	-32.72+j39.95	-32.72-j39.95	-.09+j0
-1.125	-32.74+j39.78	-32.74-j39.78	-0.11+j0
-1.433	-32.76+j39.54	-32.76-j39.54	-0.37+j0
-1.826	-32.78+j39.25	-32.78-j39.24	-0.71+j0
-2.326	-32.81+j38.86	-32.81-j38.86	-1.14+j0
-2.962	-32.84+j38.35	-32.84-j38.35	-1.71+j0
-3.774	-32.86+j37.68	-32.86-j37.68	-2.46+j0
-4.807	-32.86+j36.79	-32.86-j36.79	-3.47+j0
-6.124	-32.81+j35.59	-32.81-j35.59	-4.85+j0
-7.801	-32.66+j33.93	-32.66-j33.93	-6.80+j0
-9.937	-32.23+j31.54	-32.23-j31.54	-9.74+j0
-12.66	-31.01+j27.93	-31.01-j27.93	-11.48+j0
-16.12	-26.18+j22.73	-26.18-j22.73	-27.87+j0
-20.54	-47.81+j0	-18.37-j23.83	-18.37-j23.83
-26.16	-61.49+j0	-14.27-j26.51	-14.27-j26.51
-33.33	-74.16+j0	-11.43-j28.89	-11.43-j28.88
-42.46	-87.51+j0	-92.12-j31.05	-9.21-j31.05
-54.09	-102.51+j0	-73.88-j33.04	-7.39-j33.04
-68.90	-120.00+j0	-58.68-j34.90	-5.87-j34.90

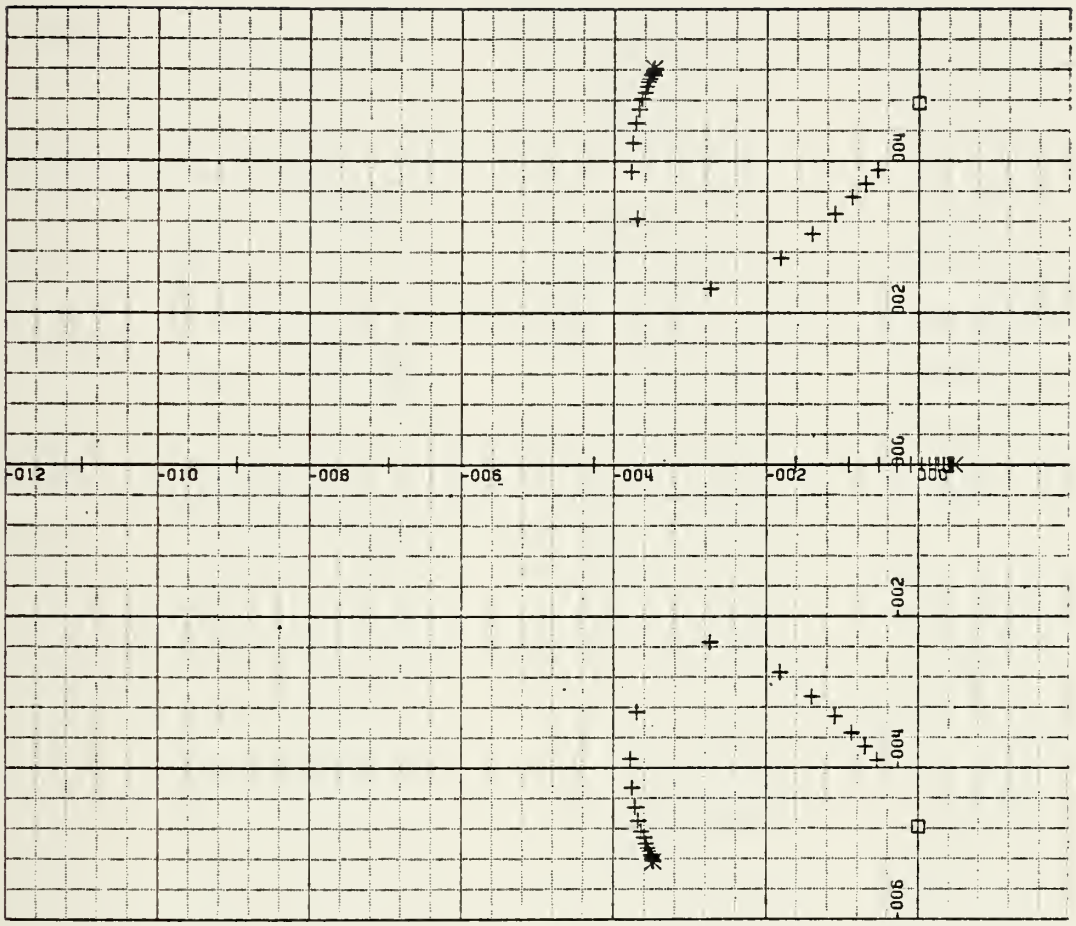

X-SCALE=2.00E+01 UNITS INCH.
Y-SCALE=2.00E+01 UNITS INCH.
ROOT LOCUS PLOT FOR MODIFIED
PRESSURE ONLY LINEAR MODEL

Figure 14

TABLE VI

Roots For Modified Pressure Lift Only Model, g_{11}=-1688, g_{12}=119, g_{13}=-18.3(varies)

k_6	A	B	C
-0.099	-34.66+j52.35	-34.66-j52.35	4.817+j0.0
-0.127	-34.68+j52.29	-34.68-j52.29	4.751+j0.0
-0.162	-34.69+j52.27	-34.69-j52.27	4.733+j0.0
-0.207	-34.70+j52.25	-34.70-j52.25	4.709+j0.0
-0.263	-34.72+j52.22	-34.72-j52.22	4.680+j0.0
-0.335	-34.73+j52.19	-34.73-j52.19	4.642+j0.0
-0.427	-34.75+j52.15	-34.75-j52.15	4.594+j0.0
-0.544	-34.78+j52.09	-34.78-j52.01	4.533+j0.0
-0.693	-34.81+j52.02	-34.81-j52.02	4.454+j0.0
-0.883	-34.85+j51.93	-34.85-j51.93	4.355+j0.0
-1.125	-34.91+j51.81	-34.91-j51.81	4.227+j0.0
-1.433	-34.98+j51.66	-34.98-j51.66	4.064+j0.0
-1.827	-35.06+j51.46	-35.06-j51.46	3.854+j0.0
-2.326	-35.17+j51.21	-35.17-j51.21	3.585+j0.0
-2.962	-35.31+j50.89	-35.31-j50.89	3.240+j0.0
-3.773	-35.48+j50.46	-35.49-j50.46	2.794+j0.0
-4.807	-35.70+j49.91	-35.70-j49.91	2.216+j0.0
-6.124	-35.97+j49.19	-35.97-j49.19	1.463+j0.0
-7.801	-36.29+j48.22	-36.29-j48.22	0.472+j0.0
-9.937	-36.67+j46.91	-36.67-j46.91	-0.849+j0.0
-12.66	-37.10+j45.11	-37.10-j45.11	-2.648+j0.0
-16.12	-37.52+j42.55	-37.52-j42.55	-5.191+j0.0
-20.54	-37.74+j38.72	-37.74-j38.72	-9.056+j0.0
-26.16	-36.96+j32.14	-36.96-j32.41	-16.11+j0.0
-33.33	-42.45+j0.0	-27.29+j23.37	-27.29-j23.37
-42.46	-69.58+j0.0	-18.18+j27.34	-18.18-j27.34
-54.09	-89.56+j0.0	-13.86+j30.54	-13.86-j30.54
-68.90	-109.98+j0.0	-10.88+j33.10	-10.88-j33.10

previous study, some values of g_{13} caused instability. Particularly, for $g_{13} > -9.9$, pole C was in the right half plane. The greatest sensitivity was experienced for values of g_{13} near $g_{13} = -30$. Note that the value of g_{13} chosen via Riccati will cause stable operation and is also removed from the value of greatest sensitivity.

3. Routh Criterion

The Routh criterion was applied in order to confirm the range of feedback gains for stable operation obtained from the root locus study. The Routh array is set up below. The C.E., given in Eq. 4.B.17, is used with the understanding that all coefficients are absolute values.

1	$a_{21} + a_{23} g_2$
$a_{33} + g_3$	$(-a_{23} g_1 + a_{21} g_3)$
$a_{21} + a_{23} g_{12} + \frac{a_{23}g_{11} - a_{21}g_{13}}{a_{33}+g_3}$	0
$-a_{23}g_1 + a_{21}g_3$	0

The conditions for stability are:

1) $g_3 > -a_{33}$ (4.B.14)

since $a_{33} = 64.493$, then

$g_3 > -64.493$ for stable operations.

2) $a_{21}g_3 > a_{23}g_1$

$$g_1 < \frac{a_{21}}{a_{23}}\ g_3 \qquad (4.B.15)$$

$$g_1 < \frac{2267.782}{11.248}\ g_3$$

$$g_1 < 201.616\ g_3$$

$$g_1 < (201.616)(-64.493)$$

$$g_1 < -13002,821$$

3) $a_{21} + a_{23}\ g_2 > -\left(\frac{a_{23}g_1 - a_{21}g_3}{a_{23}+g_3}\right)$

$$g_2 > \frac{-\left(\frac{a_{23}g_1 - a_{21}g_3}{a_{33}+g_3}\right) - a_{21}}{a_{23}}$$

$$g_2 > \frac{-\left(\frac{a_{23}g_1 - a_{21}g_3}{a_{23}+g_3}\right) - \left(\frac{a_{21}a_{33}+a_{21}g_3}{a_{33}+g_3}\right)}{a_{23}}$$

$$g_2 > \frac{\frac{-a_{23}g_1 + a_{21}g_3 - a_{21}a_{33} - a_{21}g_3}{a_{33}+g_3}}{a_{23}}$$

$$g_2 > \frac{\frac{-a_{33}g_1 - a_{21}a_{33}}{a_{33}+g_3}}{a_{23}}$$

$$g_2 > -\frac{(a_{33}g_1 + a_{21}a_{33})}{a_{23}(a_{33}+g_3)} \qquad (4.B.16)$$

If $g_3 \geq -64$ the $g_2 > -201.72$.

The boundary limits of g_2, and therefore g_1, are very sensitive to g_3.

For the specific control chosen in Section IVA, the Routh array was used to determine the stability limit for the gains.

From Eq(4.B.14)

$$g_{13} > -a_{33}$$

therefore $18.3 > -64.493$

From Eq(4.B.15)

$$g_{11} > \frac{a_{21}}{a_{23}} g_{13}$$

therefore $1688 < 3689.581$

From Eq(4.B.16)

$$g_2 > -\frac{(a_{33}g_{11}+a_{21}a_{33})}{a_{23}(a_{33}+g_{13})}$$

therefore $119 > -273.95$

It was seen from this study that the gains were well within the limits of stability. Lower gains were realitively more stable.

V. CONCLUSION

It has been shown that the linear regulator design can be applied to the problem of vertical plane motion for the captured air bubble surface effect ship. The linear pressure lift only model, developed from the simplified equations of motion, was shown to be a valid model which could be used for control analysis and design. An optimal control was found, based upon a quadratic cost function, using empirically derived weighting factors. The pressure lift only linear system showed a reduction in center of gravity acceleration for $17 < \omega_e < 100$ radians/sec. A C.G. acceleration reduction was observed in both the linear and nonlinear systems. The shape of the frequency response magnitude curves were identical. A 13% maximum reduction was observed at $\omega_e = 45$ rad/sec. where peak acceleration occurs.

The control gains derived, as shown in Section IV, are within the airflow rates currently available for the XR-3. The Riccati equation computer program on Ref. 10 proved to be a most useful tool, which facilitated experimentation of a large number of weighting coefficients, making an optimal control design more feasible.

Finally, the analysis shows that the system is stable over the range for the control gains selected. It was seen from the root locus study that the limits of stability narrowed, that the sensitivity to air flow rates increased and C.G.

acceleration decreased with higher control gains. It was seen that for these higher gains the C.G. acceleration was not reduced and the control, ∂_u, increased for ω_e<17 rad/sec. This was due to the fact that the buoyancy effects are predominant in that frequency range and the buoyancy terms are at a constant steady state value in this model.

Though an optimal control was found based on a particular quadratic cost function, many other possibilities exist. Different defined weighting factors can be experimented with, and some may result in improved C.G. reduction. The limiting factor in such a design is equipment limitation. The choice of weighting factors, and ultimately, the control, are eventually determined by that fact.

VI. RECOMMENDATIONS FOR FURTHER STUDY

The following list of recommendations is presented for consideration and further study.

A. A more realistic system presentation could be accomplished if pitch coupling was combined into the linear regulator study. This would facilitate the speed analysis study for the avoidance of wet decks and undesirable pitch accelerations.

B. The passive control technique discussed by Boggio in Ref. 6 should be examined further. The introduction of a flexible membrane into the plenum chamber may reduce vertical accelerations. This technique has been examined in model towing tank studies.

C. Since the mass of plenum air X3 cannot be directly measured, an observer might be used in conjunction with state X3 or perhaps remodel using low order model analysis. Perhaps consideration should be given to a design using only X1 and X2 as states to be used for feedback.

D. The linear regulator technique design approach should be compared in greater detail to the filter design technique proposed by Rohr Marine Inc. in Ref. 3. A fixed air flow rate, based upon a filtered observed sea state, could be a more realizable design in terms

of the physical equipment limitations. The study of fixed air flow, of Appendix E, shows that the filter design approach may offer greater control over the entire encounter frequency range. (see Fig. E-1)

APPENDIX A

The simplified non linear system of Ref. 1 is shown in Fig. A1. This system, with the buoyancy term removed, served as the basis for study in this thesis. The linearization and resultant linear system matrix is shown for the simplified non linear system. The pressure lift only model linearization is also shown.

LINEARIZATION OF THE SIMPLIFIED MODEL

The equations of motion are linearized using Taylor series expansion around the steady state operating point.

Heave acceleration:

$$\ddot{Z} = \left(\frac{W}{M} - \frac{F_p}{M} - \frac{F_l}{M}\right)$$

$$\dot{Z}(0) + \dot{\partial Z} = \frac{W}{M} - \left[\frac{F_p(0)}{M} + \frac{\partial F_p}{M}\right] - \left[\frac{F_l(0)}{M} + \frac{\partial F_l}{M}\right]$$

$$\dot{\partial Z} = -\frac{\partial F_p}{M} - \frac{\partial F_l}{M}$$

In a similar manner

$$\dot{\partial V}_m = -(nk_q)\,\partial \bar{P}_b - \frac{C_n A_1}{P_a}\left(\frac{P_a}{2\bar{P}_b(0)}\right)^{1/2} \partial \bar{P}_b$$

$$\partial F_p = A_b\,\partial \bar{P}_b$$

$$\partial F_l = (2A_s \rho_w g)\,\partial l_d$$

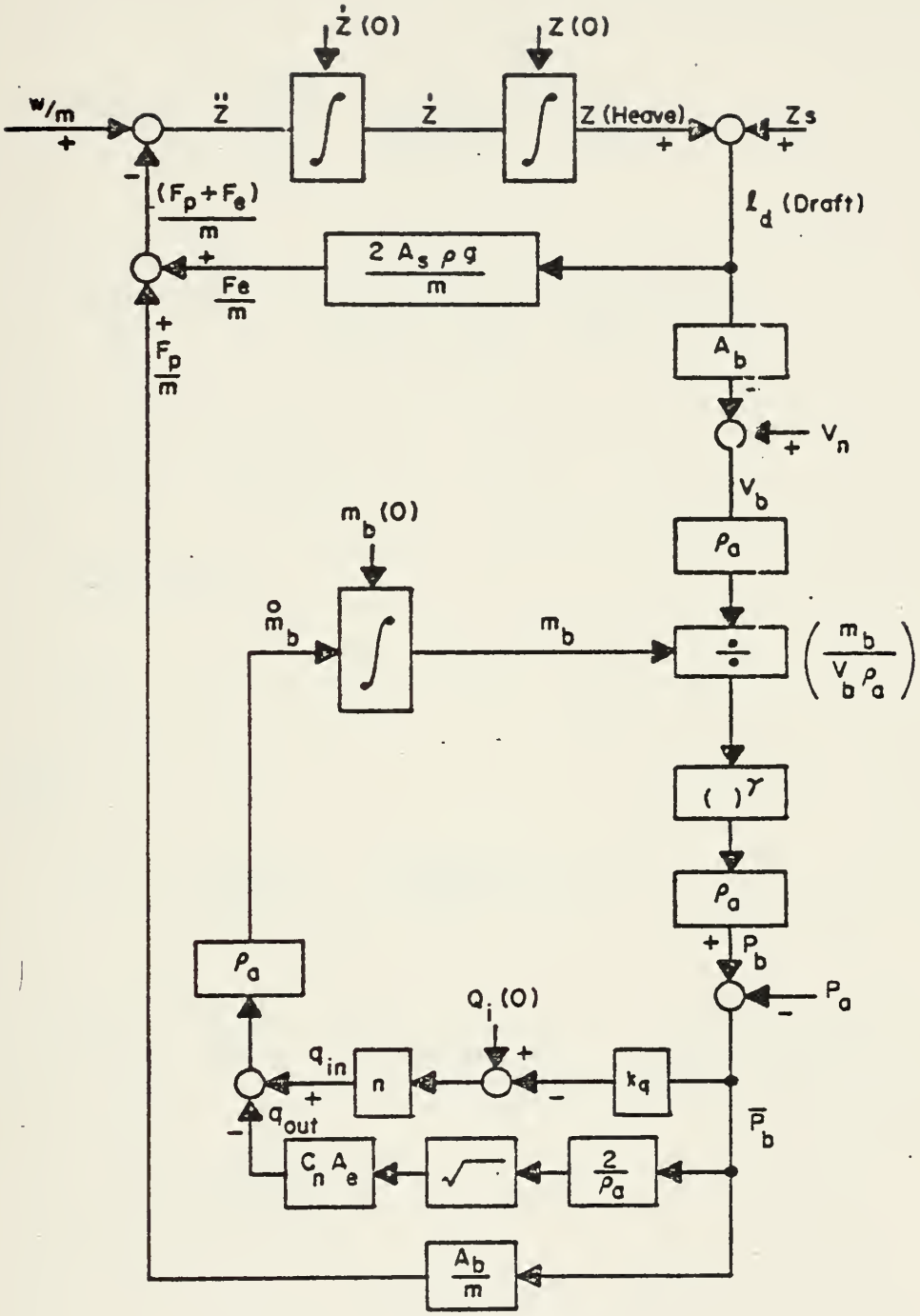

Schematic Diagram of Signal Flow.

Figure A1

$$\partial q_{in} = -(n_{kq})\,\partial \bar{P}_b$$

$$\partial q_{out} = -\frac{C_n A_1}{\rho_a}\left(\frac{\rho_a}{2\bar{P}_b(0)}\right)^{1/2}\partial \bar{P}_b$$

$$\partial P_b = \gamma P_b(0)\left[\frac{1}{V_m(0)}\,\partial V_m - \frac{1}{V_b(0)}\,\partial V_b\right]$$

$$\partial V_b = -(A_b)\,\partial l_d$$

$$\partial \bar{P}_b = \partial P_b$$

$$\partial l_d = \partial_z$$

Combining

$$\ddot{\partial Z} = -\left(\frac{A_b}{M}\right)\partial \bar{P}_b - \left(\frac{2A_s \rho_w g}{M}\right)\partial Z$$

$$\dot{\partial Z} = -\frac{A_b}{M}\left[\gamma P_b(0)\left[\frac{1}{V_m(0)}\,\partial V_m - \frac{1}{V_b(0)}(-A_b)\,\partial Z\right]\right]$$

$$- \left(2\,\frac{A_s \rho_w g}{M}\right)\partial Z$$

$$\ddot{\partial Z} = -\left[\left[\left(\frac{2A_s \rho_\omega g}{M}\right) + \left(\frac{\gamma P_b(0) A_b^{\,2}}{MV_b(0)}\right)\right]\partial Z\right.$$

$$\left. + \left[\frac{\gamma P_b(0) A_b}{MV_m(0)}\right]\partial V_m\right]$$

$$\partial\dot{V}_m = -[nk_q + \frac{C_n A_1}{\rho_a}\left(\frac{\rho_a}{2\bar{P}_b(0)}\right)^{1/2}]\,\gamma P_b(0).$$

$$\left[\frac{\partial V_m}{V_m(0)} - \frac{\partial V_b}{V_b(0)}\right]$$

$$\partial\dot{V}_m = -[n\,k_q + \frac{C_n A_1}{\rho_a}\left(\frac{\rho_a}{2\bar{P}_b(0)}\right)^{1/2}]\,\gamma P_b(0).$$

$$\left[\left(\frac{1}{V_m(0)}\right)\partial V_m + \left(\frac{A_b}{V_b(0)}\right)\partial Z\right]$$

$$\partial P_b = \gamma P_b(0)\left[\frac{1}{V_m(0)}\,\partial V_m + \frac{A_b}{V_b(0)}\,\partial Z\right]$$

The state vector is

$$\underline{X} = [\partial Z \quad \partial\dot{Z} \quad \partial V_m]^T$$

The output variable is

$$y = \partial P_b$$

$$y = C_{11}X_1 + C_{13}X_3$$

where

$$C_{11} = \frac{\gamma P_b(0) A_b}{V_b(0)}$$

$$C_{13} = \frac{\gamma P_b(0) A_b^{\,2}}{V_m(0)}$$

Writing the above equations in state equation form;

$$\dot{X}_1 = X_2$$

$$\dot{X}_2 = -[(\frac{2A_s\rho_w g}{M}) + (\frac{\gamma P_b(0)A_b^2}{M\,V_b(0)})]\,X_1$$

$$+ [-(\frac{\gamma P_b(0)A_b}{MV_m(0)})]\,X_3$$

$$\dot{X}_3 = [-\gamma P_b(0)[nk_q + \frac{C_n A_1}{\rho_a}(\frac{\rho_a}{2P_b(0)})^{1/2}]\,\frac{A_b}{V_b(0)}]\,X_1$$

$$+ [-\gamma P_b(0)[nk_q + \frac{C_n A_1}{\rho_a}(\frac{\rho_a}{2P_b(0)})^{1/2}]\frac{1}{V_m(0)}]\,X_3$$

or

$$\dot{X}_1 = X_2$$

$$\dot{X}_2 = a_{21}X_1 + a_{23}X_3$$

$$\dot{X}_3 = a_{31}X_1 + a_{33}X_3$$

The characteristic equation was found from the system matrix,

$$DET(sI-A) = 0$$

to be

$$s^3 + 62s + 2183s + 789 = 0$$

which factors into;

$$(s+.37)(s+30.82+j34,8)(s+30.82-j34,8)$$

TAYLOR SERIES EXPANSION OF PRESSURE LIFT ONLY VERTICAL EQUATIONS OF MOTION

Defining

$$W_m = \frac{W}{M}$$

$$F_{pm} = \frac{F_p}{M}$$

then incremental acceleration due to pressure is:

$$\dot{Z}(0) + \partial\ddot{Z} = \frac{W}{M} - (F_{pm}(0) + \partial F_{pm})$$

$$\partial\ddot{Z} = - \partial F_{pm}$$

Defining the air mass volume:

$$V_m = \frac{M_b}{\rho_a} = q_{in} - q_{out}$$

$$\dot{V}_m(0) + \partial V_m = nQ_{IQ} - nk_q(\overline{P_b}(0) + \partial P_b)$$

Then the incremental volumetric change in air mass is;

$$\partial \ddot{V}_m = - (nk_q) \partial \overline{P_b} - \frac{C_n A_l}{\rho_a} \left(\frac{\rho_a}{2\overline{P_b}(0)}\right)^{1/2} \partial \overline{P_b}$$

and the incremental force due to pressure is;

$$\partial F_p = A_b \partial \overline{P_b}$$

Incremental air flow into the plenum

$$\partial q_{in} = -(nk_q) \partial \overline{P_b}$$

Incremental air flow out of the plenum

$$\partial q_{out} = - \frac{C_n A_l}{\rho_a} \left(\frac{\rho_a}{2\overline{P_b}(0)}\right)^{1/2} \partial \overline{P_b}$$

Incremental gauge pressure (plenum)

$$\partial P_b = \gamma P_b(0) \left[\frac{\partial V_m}{V_m(0)} - \frac{\partial V_b}{V_b(0)}\right]$$

Incremental plenum volume

$$\partial V_b = A_b L_d$$

Incremental Pressure (plunum)

$$\partial \overline{P_b} = \partial P_b$$

Incremental Draft

$$\partial L_d = \partial Z$$

Combining

Acceleration ($\partial \ddot{Z}$)

$$\partial \ddot{Z} = - \frac{A_b}{M} \partial \overline{P_b}$$

$$= - \frac{A_b}{M} [\gamma P_b(0)[\frac{\partial V_m}{V_m(0)} - \frac{-A_b \partial Z}{V_b(0)}]]$$

$$\partial \ddot{Z} = - [\frac{\gamma P_b(0) A_b^2}{M V_b(0)}] \partial Z - [\frac{\gamma P_b(0) A_b}{M V_m(0)}] \partial V_m$$

Volumetric air mass ($\partial \dot{V}_m$)

$$\partial \dot{V}_m = -[nk_q + \frac{C_n A_1}{\rho_a}(\frac{\rho_a}{2\overline{P_b}(0)})^{1/2}]\gamma P_b(0)[\frac{\partial V_m}{V_m(0)} - \frac{\partial V_b}{V_b(0)}]$$

$$\partial \dot{V}_m = -[nk_q + \frac{C_n A_1}{\rho_a}(\frac{\rho_a}{2\overline{P_b}(0)})^{1/2}]\gamma P_b(0)[\frac{\partial V_m}{V_m(0)} + \frac{A_b \partial Z}{V_b(0)}]$$

Plenum Pressure

$$\partial P_b = \gamma P_b(0) \left[\frac{\partial V_m}{V_m(0)} + \frac{A_b}{V_b(0)} \partial Z\right]$$

A series of system coefficients, k_n, were defined for ease of writing and are used throughout the thesis. They are,

$$k_1 = \left(\frac{2W_p V_w}{\omega_i}\right) \text{Sin} \left(\frac{W_L L_p}{2V_w}\right)$$

$$k_2 = \frac{1}{V_b(0)}$$

$$k_3 = \gamma P_b(0)$$

$$k_4 = \frac{A_b}{M}$$

$$k_6 = nk_q + \frac{C_n A_1}{\rho_a} \sqrt{\frac{\rho_a}{2\bar{P}_b(0)}}$$

$$k_7 = \frac{1}{V_m(0)}$$

$$k_8 = A_b$$

k_{10} = 1 constant

APPENDIX B

A brief step weight removal study was performed and compared to Ref. 1 as an additional check on system validity. The IODE remote terminal CP-CMS program on the IBM/360 was used in this study. A sample listing is shown in Appendix C.

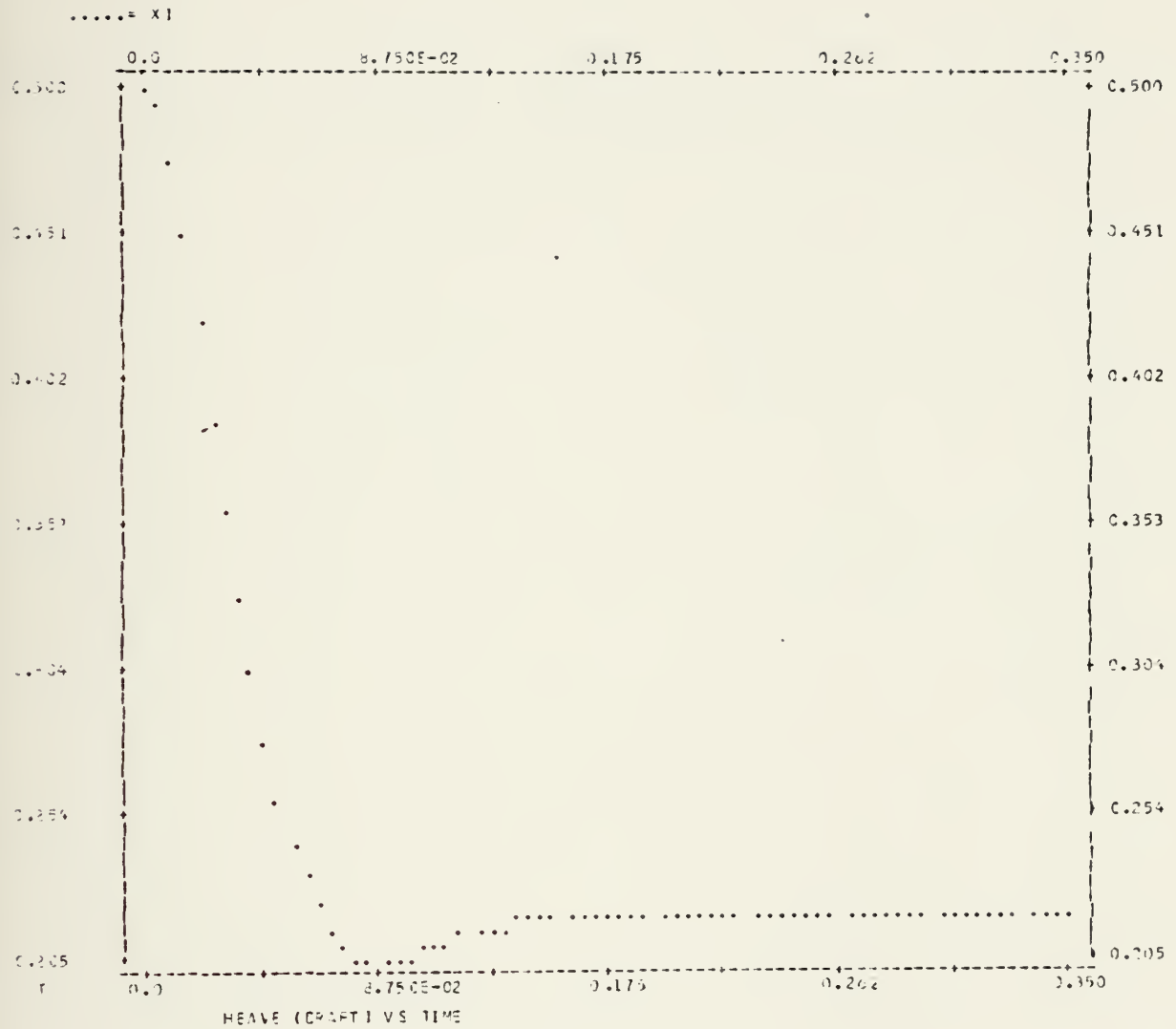
.....= X1
0.0
8.750E-02
0.175
0.262
0.350
0.500
0.451
0.402
0.353
0.304
0.254
0.205
T
HEAVE (CRAFT) VS TIME

Figure B1

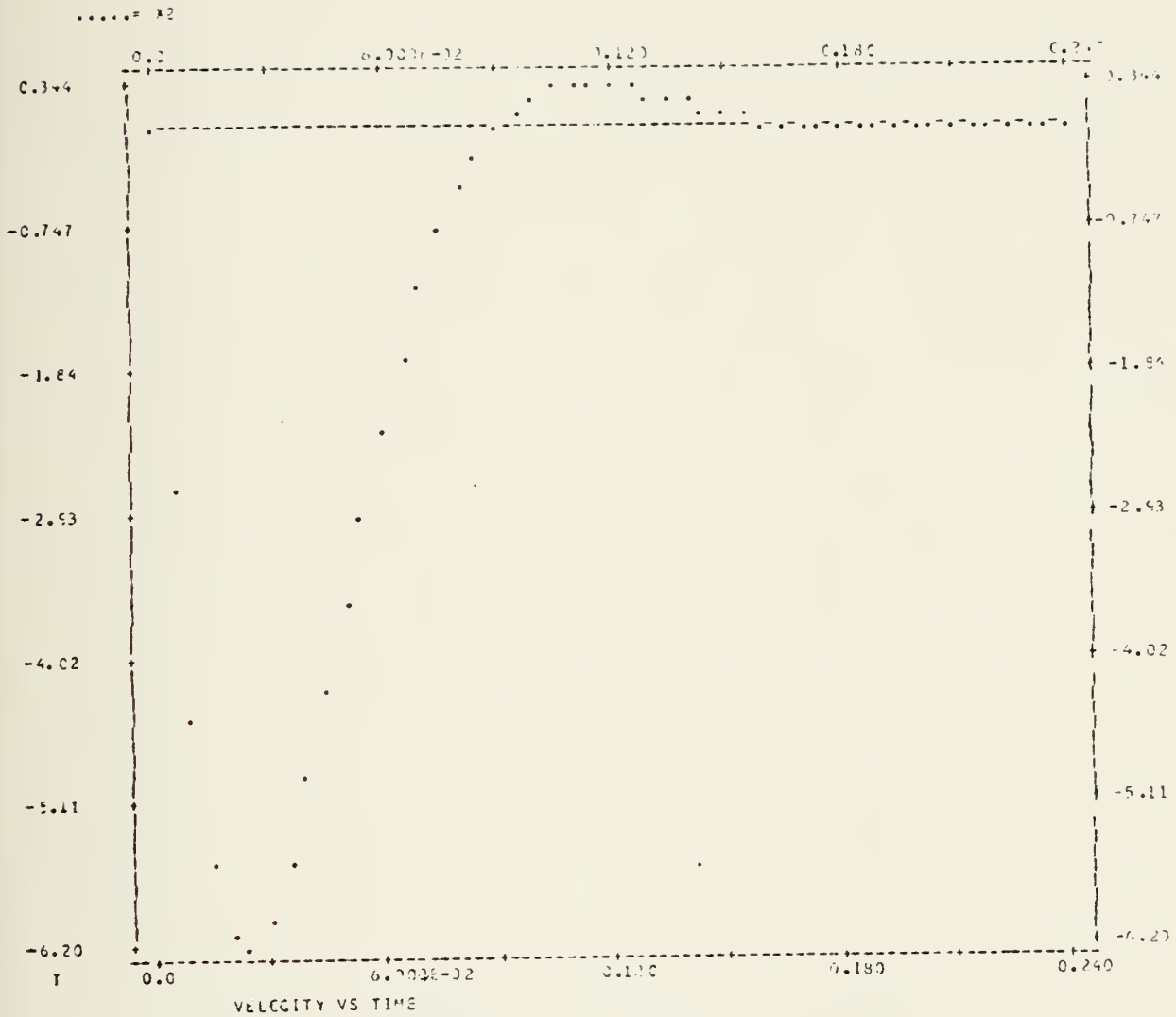

Figure B2

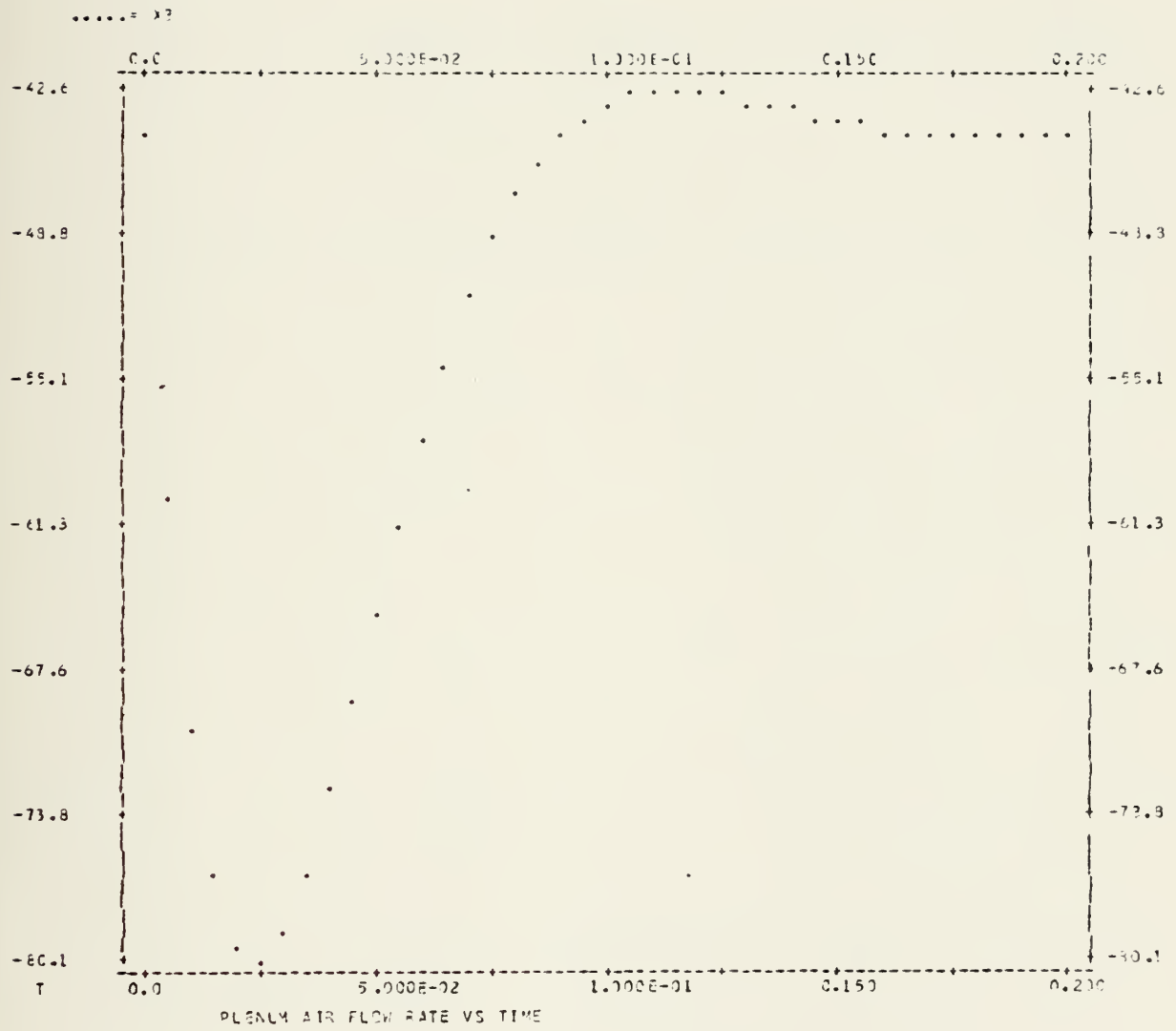
.....= X3
0.0
5.000E-02
1.000E-01
0.150
0.200
-42.6
-48.8
-55.1
-61.3
-67.6
-73.8
-80.1
T
PLENUM AIR FLOW RATE VS TIME

Figure B3

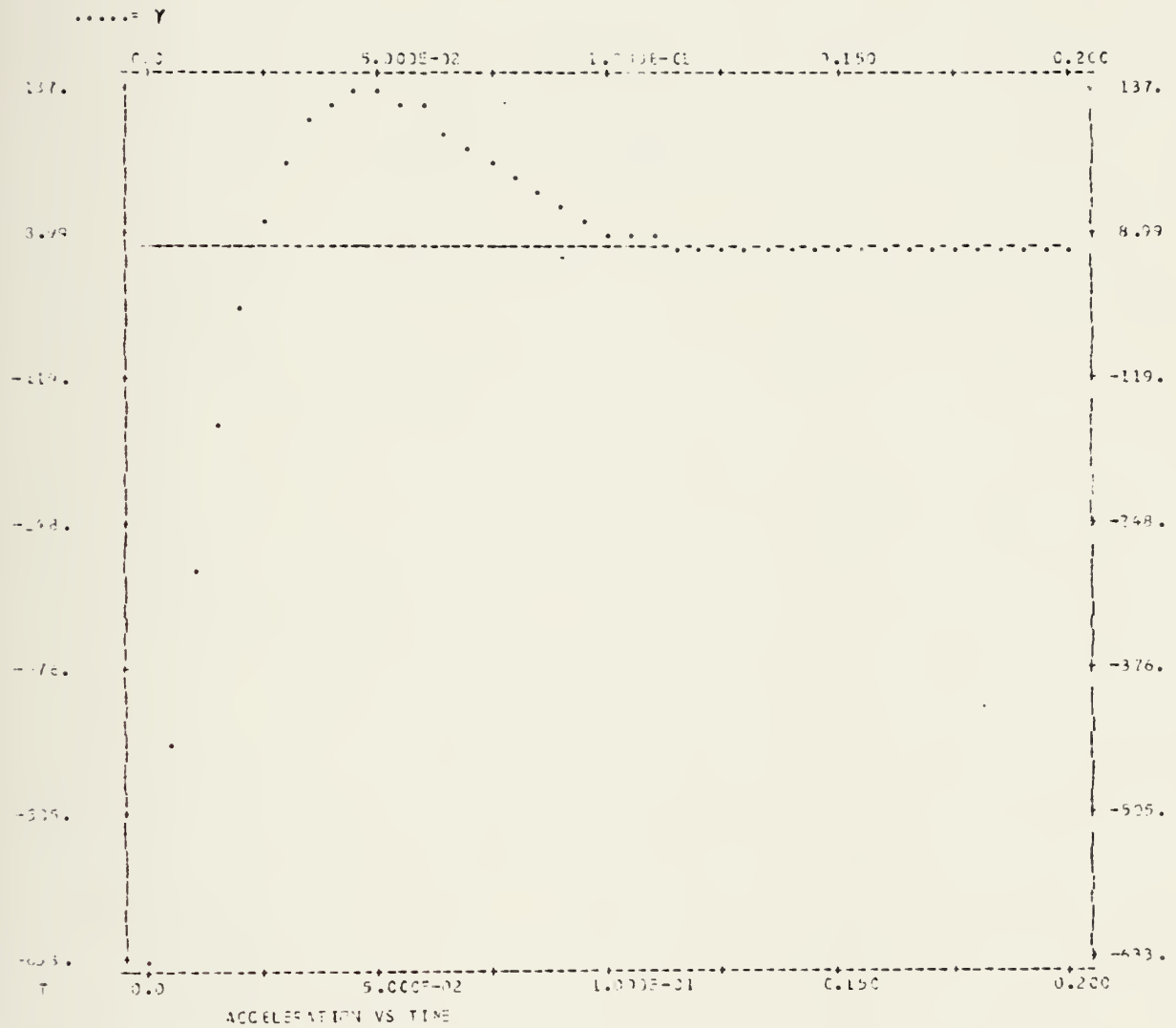
..... Y
0.0
5.0000E-02
0.150
0.200
137.
8.99
-119.
-248.
-376.
-505.
-633.
T
0.0
5.0000E-02
0.150
0.200
ACCELERATION VS TIME

Figure B4

APPENDIX C

The following are the listings for the various computer programs used in the preparation of this thesis.

```
//  JX C LTUCCA
//LINK.SYSUT1 DD
S    D  LIB  ,  CARD
   INCLUDE SYSLIB(PROCATT)
//GO.SYSIN DD *
FLEXV  CANTILEVER BEAM
SYSTEM MATRIX
0.0             1.0             0.0
-2267.762       0.0             -11.248
-13722.9        0.0             -64.493
B  MATRIX
0.0             0.0             1.0
OUTPUT MATRIX
-2267.762       0.0             -11.248
0               1.0             2.0
D  MATRIX
.03
G  MATRIX
1000000.        0.0             0.0
0.0             1000.           0.0
0.0             0.0             .5
STORED W AND R MATRICES FOR TRANSIENT SOLUTION
0               0.0             21.0        023
.03
1000000.        0.0             0.0
0.0             1000.           1.0
0.0             0.0             .5
BLANK CARD
BLANK CARD
BLANK CARD
```

```
//  X C DSL
//PLOT.INPUT DD *
C**L    **  S  S  STABILITY TESTS **
I NCL  .PLOT
CONST  NPLOT=3
D      COMPLEX S,D,A,G,H
D      COMMON /CAPA/S,D,A,G,H
CONST  A=2267.782
CONST  CR=57.174
PARAM  K6=6.14422
DYNAMIC
       LOGW=AMPC(0.)
       W=10.**LOGW
       S=CMPLX(0.,W)
       V=(2.*3.14159*CR)/W
       X=62.8319/V
       K=-A*(SIN(X))/X
       N=-A*(S**2)
       D=(S**2)+(1..497*K6*S)+2267.782
       G=N/D
       H=G/(1+G)
       MAG=CABS(G)
       MAGH=CABS(H)
       VDB=20.*ALOG10(MAG)
       VDBH=20.*ALOG10(MAGH)
       GAIN=LIMIT(0.0,100.0,GAIN)
       GIMAG=LIMIT(0.0,46.0,GIMAG)
       PHI180=PHI+180.
       PHIZ=-180.
       LOGL=0.
SAMPLE
       CALL DRAW(1,1,LOGW,VDB)
       CALL DRAW(1,2,LOGW,LOGL)
TERMINAL
       CALL LABPW(NPLOT)
PARAMETER 0.01,LOGW,VDB,VDBH,PHI,PHI180,GAIN,GIMAG
CONTROL MINTIM=2.0,CTLT=.005,DCLS=.005
PRINT  0.05,W,PHI,MAG,IM,VDB,MAG,VDBH,MAGH
END
PARAM  K6=12.0
END
PARAM  K6=19.0
END
STOP
//G.SYSPRINT DD SYSOUT=A,DSN=
//PLOT.SYSIN DD *
CAB  SAS  K6=6.14422
BODE  PLOT, MAG(DB) VS. LOG W
CAB  SAS  K6=12.0
BODE  PLOT, MAG(DB) VS. LOG W
CAB  SAS  K6=19.0
BODE  PLOT, MAG(DB) VS. LOG W
```

```
//  X C CSL
//L.  PLOT DD *
TITL  ** CL CAB S C SIMULATION **
INTE  PLOT
CO  T PLOT=6
CONTROL PRINT=.5, D LT=.005, D LS=.005
PRINT .005,Z2DOT
PARAM W =51.
INITIAL
      Z=.0
      VS=75.
      SHCG=1.99
      G=32.174
      FL=(2.*VS*SHCG*G*(.5))/4.
      RHO=.00238
      AB=200.
      M=5.
      CN=.9
      PA=2116.
      W=6007.
      M=W/G
      CABL=((-W/M)+(FL/M))/(-AB/M)
      KG=1.
      GIC=6 .0
      G=M*(GIC-KG*PBBI)
      AL=Q/(CN*SQRT((2.*PBBI)/RHO))
      VM=983.
      GAM=1.4
      ZS=2.5
      MBC=2.*RHO*(((PBBI+PA)/PA)**(1./GAM))
      K1=19.3044
      LM=(2.*3.14159265*G)/MB
      TH TA=(3.14159265*KN)/LM
      K1=AB*((SIN(TH TA)))/TH TA
DERIVATIV
      TIM=A*SIN(W*TIME)
      LD=ZS+Z
      VB=VM-(AB*LD)-(K1*(TA))
      PB=PA*(MB/(VB*RHO))**GAM
      PBB=PB-PA
      APBB=ABS(PBB)
      GOLT=(CN*AL)*(SQRT((2.*APBB)/RHO))*(APBB/PBB)
      GIN=M*(GIC-KG*PBB)
      Z2DOT=-(AB/M)*PBB+(W/M)-(FL/M)
      MBDOT=RHO*(GIN-GOLT)
      ZDOT=INTGRL(0., Z2DOT)
      Z=INTGRL(-2.0,ZDOT)
      MB=INTGRL(MBO, MBDOT)
TERMINAL
      CALL  NDFW(1,PLOT)
END
PARAM W =51.
END
PARAM W =39.
END
PARAM W =38.
END
PARAM W =33.
END
PARAM W =31.
END
STOP
//G.SYSPRINT DD SYSOUT=A,DSN=
```

```
     OPTIMAL CONTROL/KALMAN FILTER PROGRAM
     PROBLEM IDENTIFICATION - HEAVE CONTROL
**********************************************
      THE A MATRIX
     0.0                  1.0000000000 00       0.0
    -2.2677820000 03      0.0                  -1.1248000000 01
    -1.3002600000 04      0.0                  -6.4493000000 01
      THE B MATRIX
     0.0                  0.0                   1.0000000000 00
      THE C MATRIX
    -2.2677820000 03      0.0                  -1.1248000000 01
**********************************************
     *** CONTROL OPTION ***

      THE R MATRIX
     3.0000000000-02
      THE C MATRIX
     1.0000000000 05      0.0                   0.0
     0.0                  1.0000000000 03       0.0
     0.0                  0.0                   5.0000000000-01
     STEADY STATE SOLUTION
      GAINS
     1.6880946900 03     -1.1911560600 02       1.8305782600 01
**********************************************
     *** CONTROL OPTION ***

      THE R MATRIX
     3.0000000000-02
      THE Q MATRIX
     1.0000000000 05      0.0                   0.0
     0.0                  1.0000000000 03       0.0
     0.0                  0.0                   5.0000000000-01
      INITIAL CONDITIONS
     0.0                  0.0                   0.0
     0.0                  0.0                   0.0
     0.0                  0.0                   0.0
**********************************************
      TIME =,      2.0000000000 01
     GAINS
     0.0                  0.0                   0.0
      TIME =,      1.9000000000 01
     GAINS
     1.6880950600 03     -1.1911557100 02       1.8305777200 01
      TIME =,      1.8000000400 01
     GAINS
     1.6880946900 03     -1.1911560600 02       1.8305782600 01
      TIME =,      1.7000000600 01
     GAINS
     1.6880946900 03     -1.1911560600 02       1.8305782600 01
      TIME =,      1.6000000800 01
     GAINS
     1.6880946900 03     -1.1911560600 02       1.8305782600 01
```

```
 THE INPUT DATA IS
GRAPH TITLE AND SCALING DATA
ROOT LOCUS PLOT FOR MODIFIED
PRESSURE ONLY LINEAR MODEL

  XSCALE     YSCALE       IXUP     IYHIGH      IWIDE      IHIGH      IGRID
    20.0       20.0          3          6          7          6          1

ORDER OF THE CHARACTERISTIC EQUATION
 3

CONSTANT PART OF THE COEFFICIENTS IN DESCENDING ORDER
0.100000 01 0.0          0.226780 04 0.570100 00

VARIABLE PART OF THE COEFFICIENTS IN DESCENDING ORDER
0.0          0.104970 02 0.0          0.0

INITIAL VALUE OF THE VARIABLE
     0.500000 01

NUMBER OF DECADES TO BE SPANNED
 1
THE SYSTEM POLES ARE
*** I M S L(UERTST) ***  WARNING(WITH FIX)       ZQADR      2 (IER =  66)
REAL PART

   0.125700-03     0.125700-03    -0.251395-03
IMAGINARY PART

   0.476218 02    -0.476218 02     0.0
THE SYSTEM ZEROS ARE

REAL PART

   0.0             0.0
IMAGINARY PART

   0.0             0.0
ALL POINTS HAVE THE SAME COORDINATES.
THIS PLOT WILL NOT BE OUTPUT.
```

```
-----SPECIFICATIONS-----

VARIABLES & INITIAL CONDITIONS:
X1 = 0.0
X2 = 0.0
X3 = 0.0
T = 0.0

CONSTANTS:
A21 = 2267.782000
A23 = 11.24800000
A31 = 2116.265000
A33 = 10.49700000
B21 = 2267.782000
B31 = 2116.265000
B32 = 1.000000000
G = 32.17400000
A = 0.1000000000D 00
WE = 45.50000000
K6 = 6.144220000
K11 = -1688.094700
K12 = 119.1160000
K13 = -18.30600000

SPECIAL FUNCTIONS:
LW = (2.*3.14159265*G)/WE
F = (SIN(62.8319/LW))/(62.8319/LW)
SEA = A*SIN(WE*T)
U2 = K11*X1+K12*X2+K13*X3
Y = -A21*X1-A23*X3-B21*F*SEA

DERIVATIVES:
D(X1 )/D(T ) = =
    X2
D(X2 )/D(T ) = =
    -A21*X1-A23*X3-B21*F*SEA
D(X3 )/D(T ) = =
    -A31*K6*X1-A33*K6*X3-B31*K6*F*SEA+U2

OUTPUTS:
   TITLE: CAB SES INCREASED AIR FLOW RATE
   TABULATE: T        Y
      AT INTERVAL    0.5000000000D-02
   NO PLOTTING

END CALCULATION WHEN T .GE. 1.50000
```

```
-----SPECIFICATION-----

VARIABLES & INITIAL CONDITIONS;
X1 = 0.500000
X2 = 0.0
X3 = -44.5300
T = 0.0

SPECIAL FUNCTIONS:
Y = 2030.26*X1_10.09*X3

DERIVATIVES:
D(X1 /D(T ) = =
    X2
D(X2 /D(T ) = =
    -2182.68*X1-10.76*X3
D(X3 /D(T 0 = =
    -12504.36*X1-62.0*X3

OUTPUTS:
   TITLE:  SES
   TABULATE:  T      X1      X2      X3      Y
      AT INTERVAL   0.300000D-01
   PLOT:  X2
      AGAINST:  T     AT INTERVAL   0.100000D-01

END CALCULATION WHEN T .GE. 0.600000
```

APPENDIX D

The characteristic equation for the pressure lift only model under control conditions was derived from the system matrix with the feedback control gains added to the state X_3. The result was compared with the characteristic equation of Section IV.B.1.

The system matrix is

$$A = \begin{bmatrix} 0 & 1 & 0 \\ a_{21} & 0 & a_{23} \\ a_{31} & 0 & a_{33} \end{bmatrix}$$

and with feedback gains;

$$A = \begin{bmatrix} 0 & 1 & 0 \\ a_{21} & 0 & a_{23} \\ a_{31}+g_{11} & +g_{12} & a_{33}+g_{13} \end{bmatrix}$$

The characteristic equation with gains becomes

$$s^3-(a_{33}+g_{13})s^2-(a_{23}g_{12}+a_{21})s$$

$$-a_{23}a_{31}-a_{23}g_{11}$$

$$+a_{21}a_{33}+a_{21}g_{13}$$

It should be noted that the above equation is identical to that derived in Ref. 1 except that the gains are shown in (4.B.4)

$$a_{21} = -2267.782$$

$$a_{23} = -11.248$$

$$a_{31} = -13002.8$$

$$a_{33} = -64.493$$

From the Riccati equation, it was seen that the gains had the following sign values;

$$-g_{11} \; , \quad +g_{12} \; , \; -g_{13}$$

Substitution of the appropriate signs yields

$$s^3+(a_{33}+g_{13})s^2+(a_{23}g_{12}+a_{21})s$$

$$+a_{21}a_{33}+a_{21}g_{13}$$

$$-a_{23}a_{31}-a_{23}g_{11}$$

Substituting in the system value parameters, the characteristic equation becomes:

$$s^3+(64.493+g_{13})s^2+(2267.782+11.248g_{12})s-11.248g_{11}$$

$$+2267.782g_{13} + .5710$$

APPENDIX E

FIXED AIR FLOW RATE STUDY

A brief study was conducted to examine the effects of k_6 on the overall frequency response and compared with the optimal control design results. Earlier work indicated that the system response was sensitive air flow rate. Therefore three values of k_6 were tested on the pressure lift only non linear system with the resultant response curves plotted. Values for k_6 are:

$k_6 = 6.144$, Fig. E1

$k_6 = 12.0$, Fig. E2

$k_6 = 19.0$ m Fig. E3

Note that the high acceleration midband frequencies are attenuated as k_6 increases. The response curve flattens out and midband frequencies are reduced by 20%. This result would tend to confirm the contention, of Ref. 3, that filtered fixed air flow rates method of control may have advantages. The time response for sinusoidal input remains linear throughout the range of interest. The time versus acceleration plot shown is a time history for an air flow rate of $Q_{IO} = 60$ at an encounter frequency of ω_e=45 rad/sec. Appendix C presents the DSL Bode program listing. Finally,

the system peak frequency magnitude plot for the conditions of no control, state variable feedback control and fixed air flow rate control is shown in Fig. E8 for Q_{IO}=60.

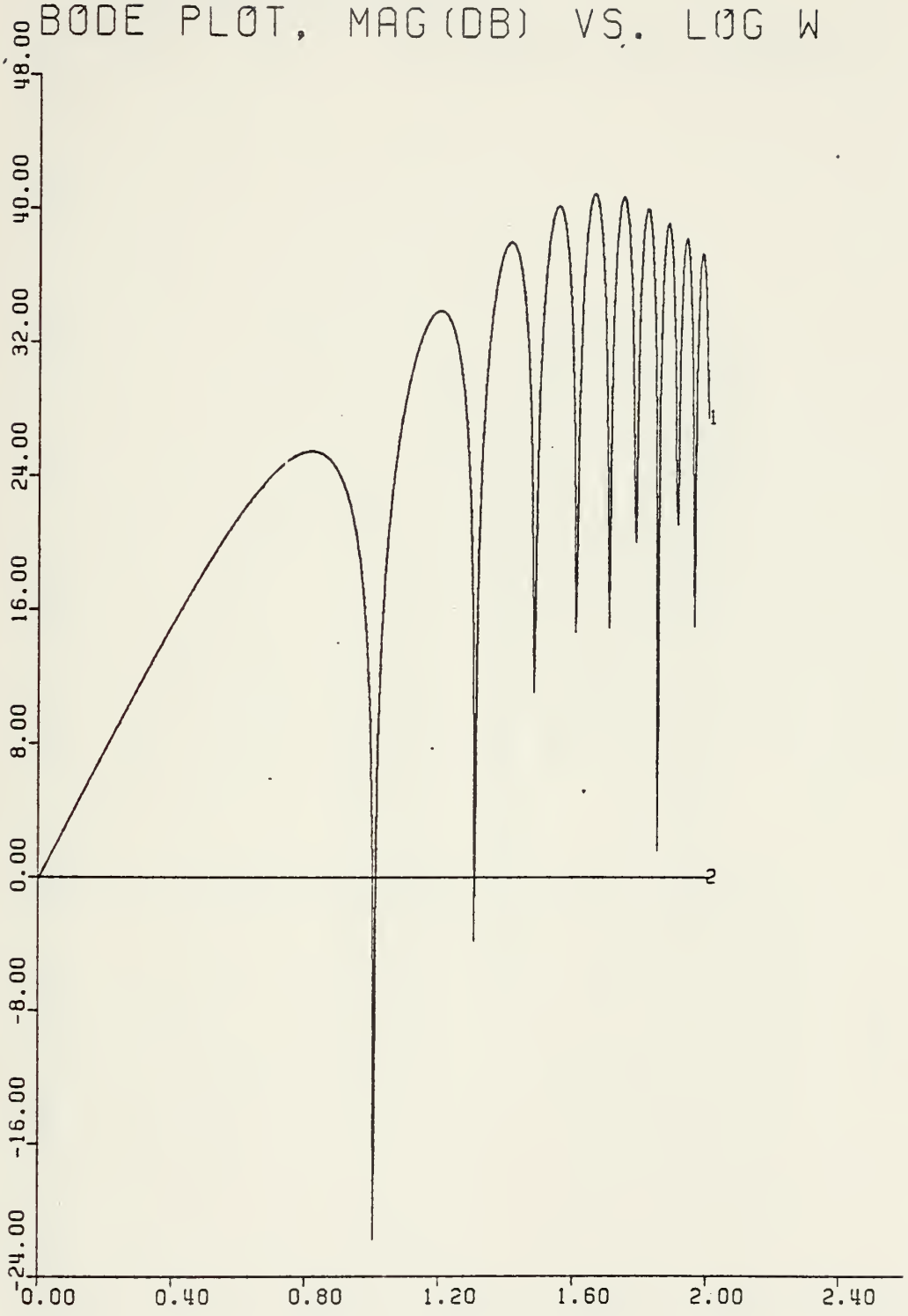

XSCALE= 0.40 UNITS/INCH
YSCALE= 8.00 UNITS/INCH

Figure E1

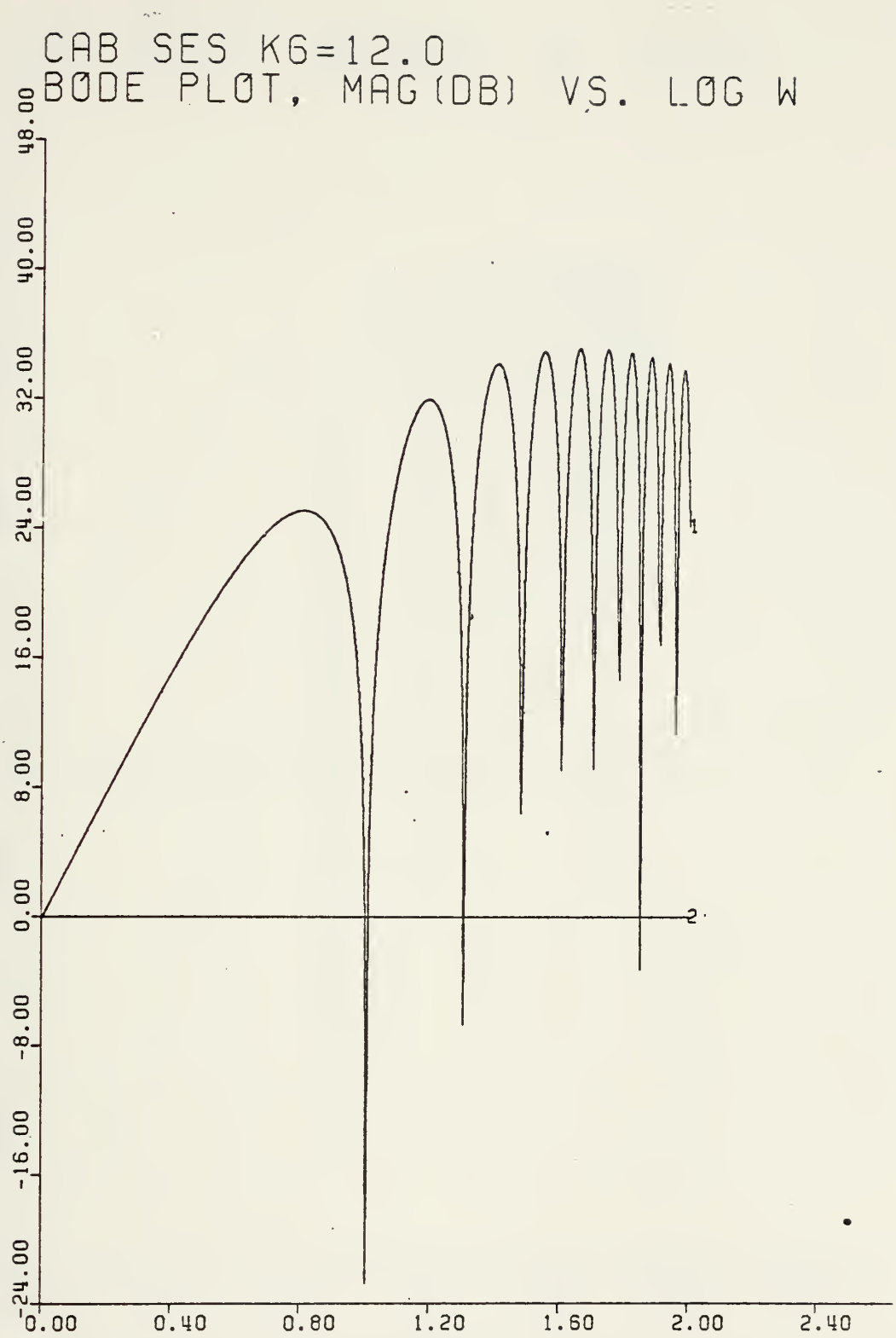

XSCALE= 0.40 UNITS/INCH
YSCALE= 8.00 UNITS/INCH

Figure E2

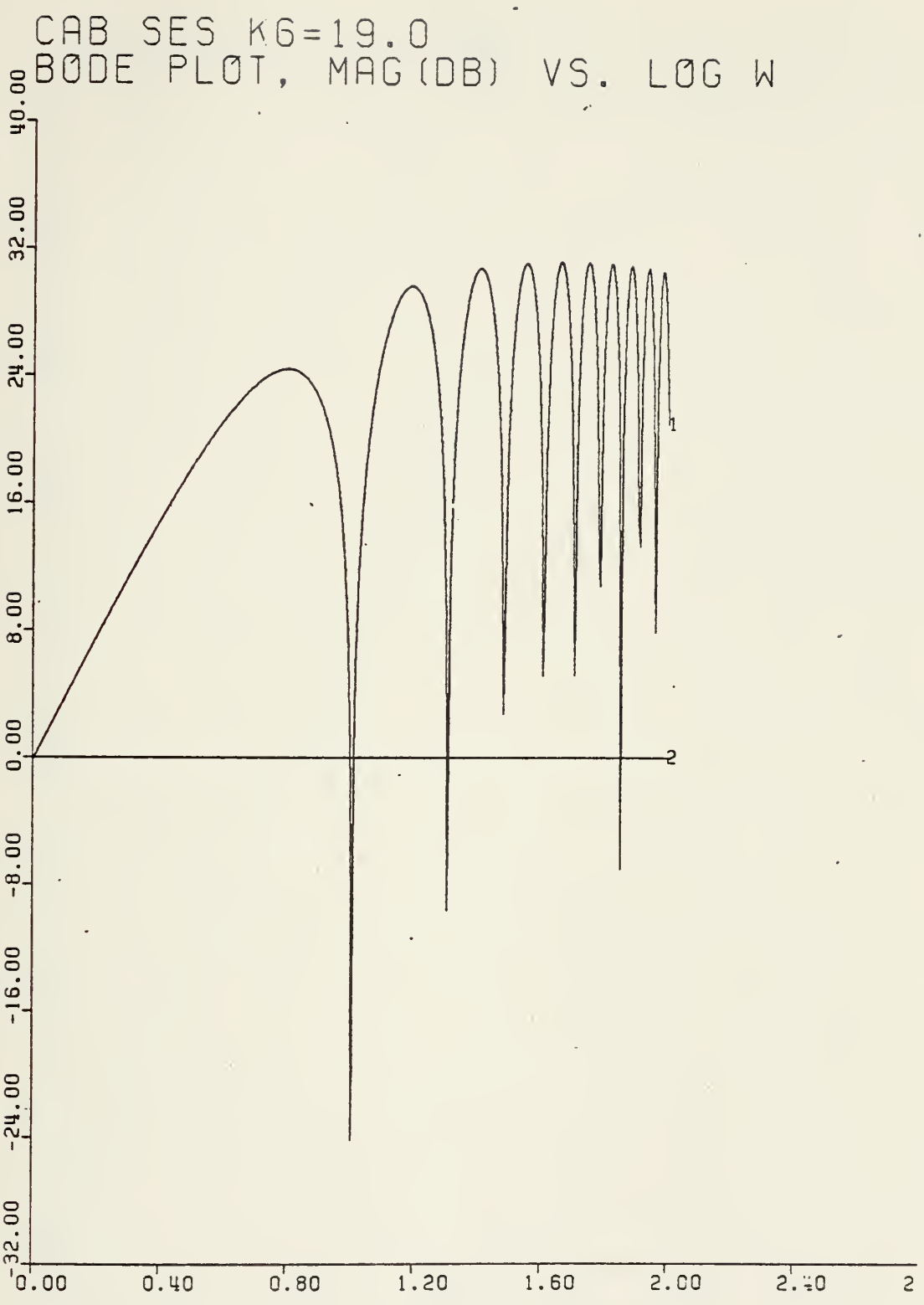

XSCALE= 0.40 UNITS/INCH
YSCALE= 8.00 UNITS/INCH

Figure E3

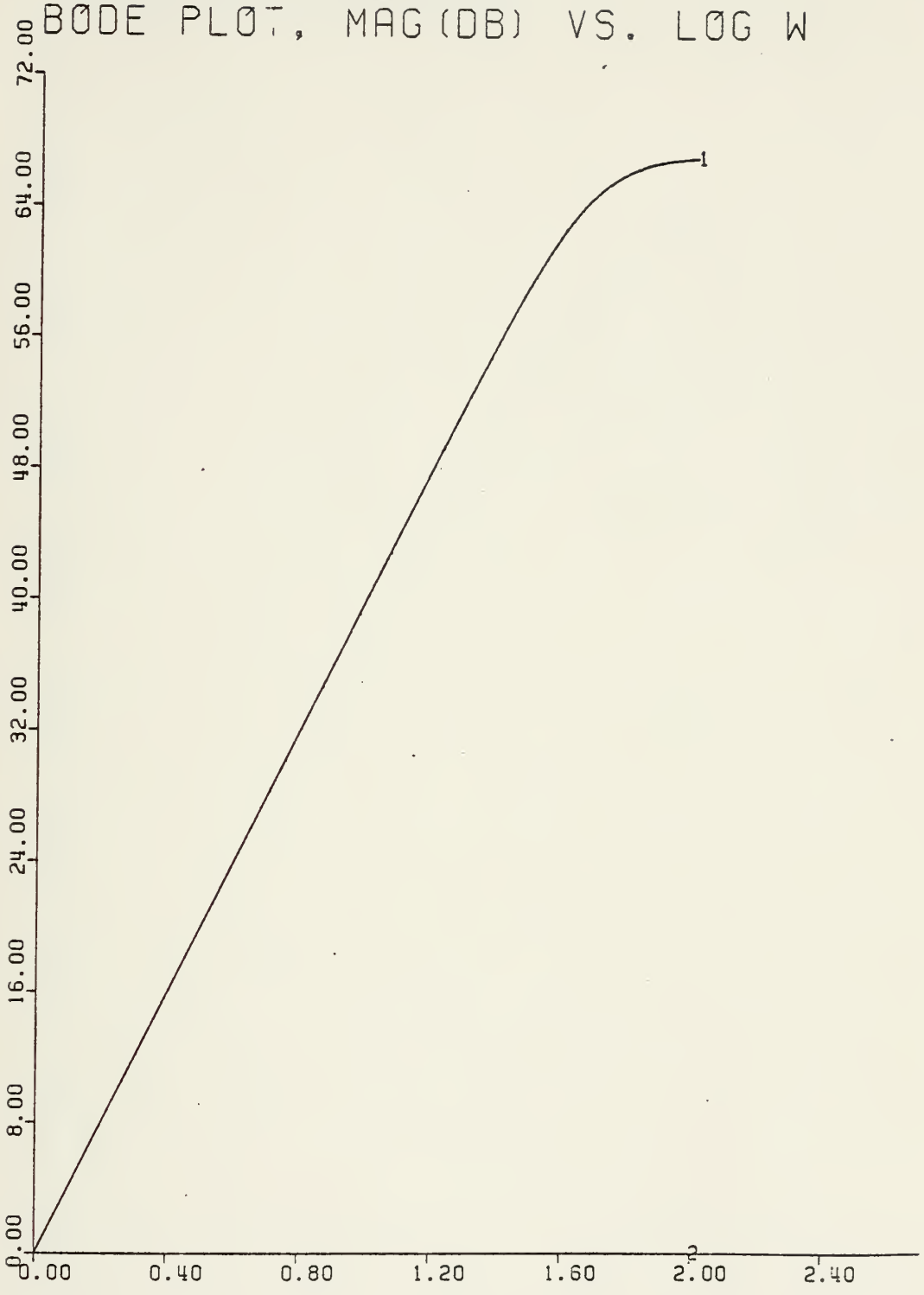

XSCALE= 0.40 UNITS/INCH
YSCALE= 8.00 UNITS/INCH

Figure E4

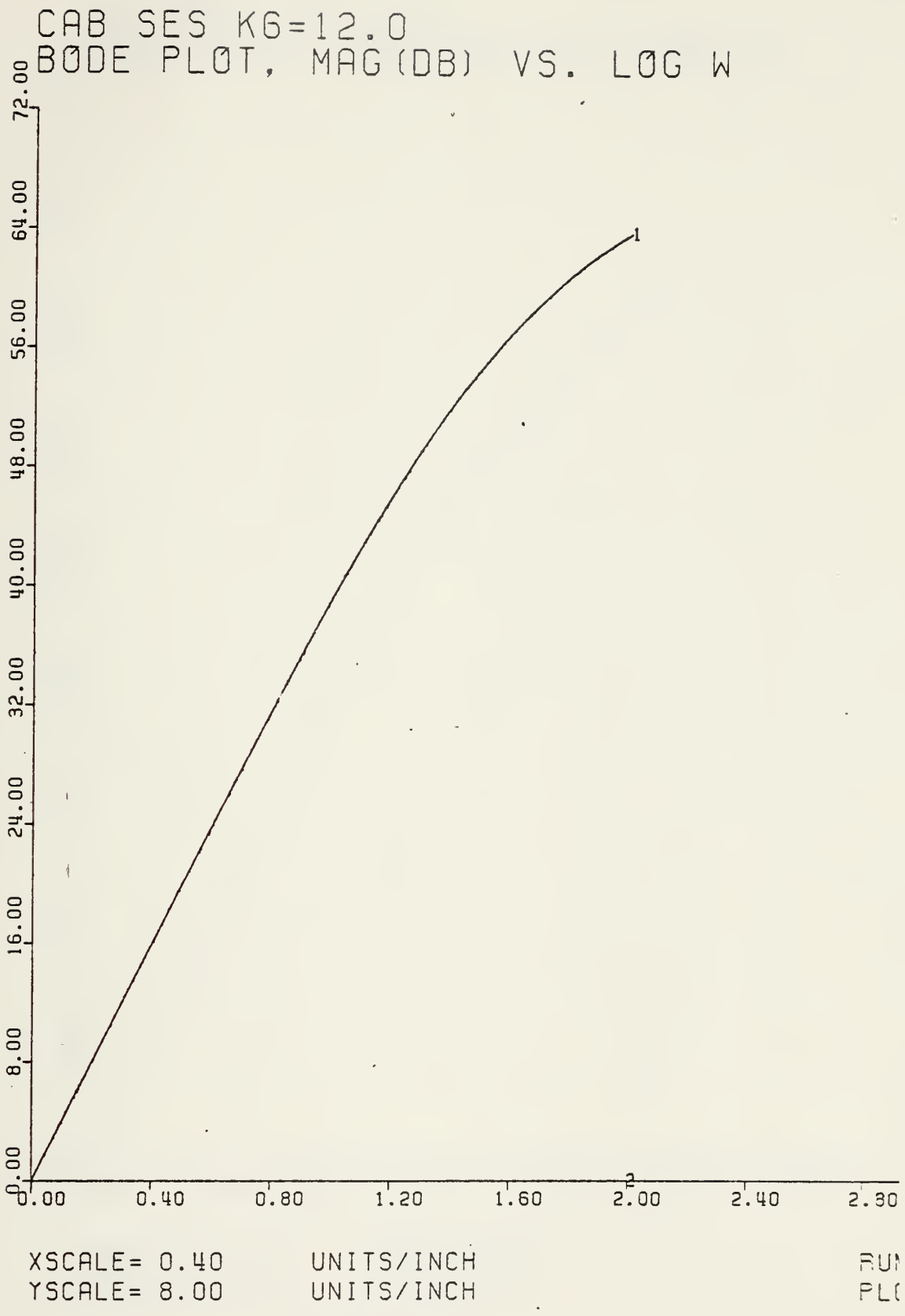
CAB SES K6=12.0
BODE PLOT, MAG(DB) VS. LOG W
72.00
64.00
56.00
48.00
40.00
32.00
24.00
16.00
8.00
0.00
0.00
0.40
0.80
1.20
1.60
2.00
2.40
2.80
1
2
XSCALE= 0.40 UNITS/INCH
YSCALE= 8.00 UNITS/INCH

Figure E5

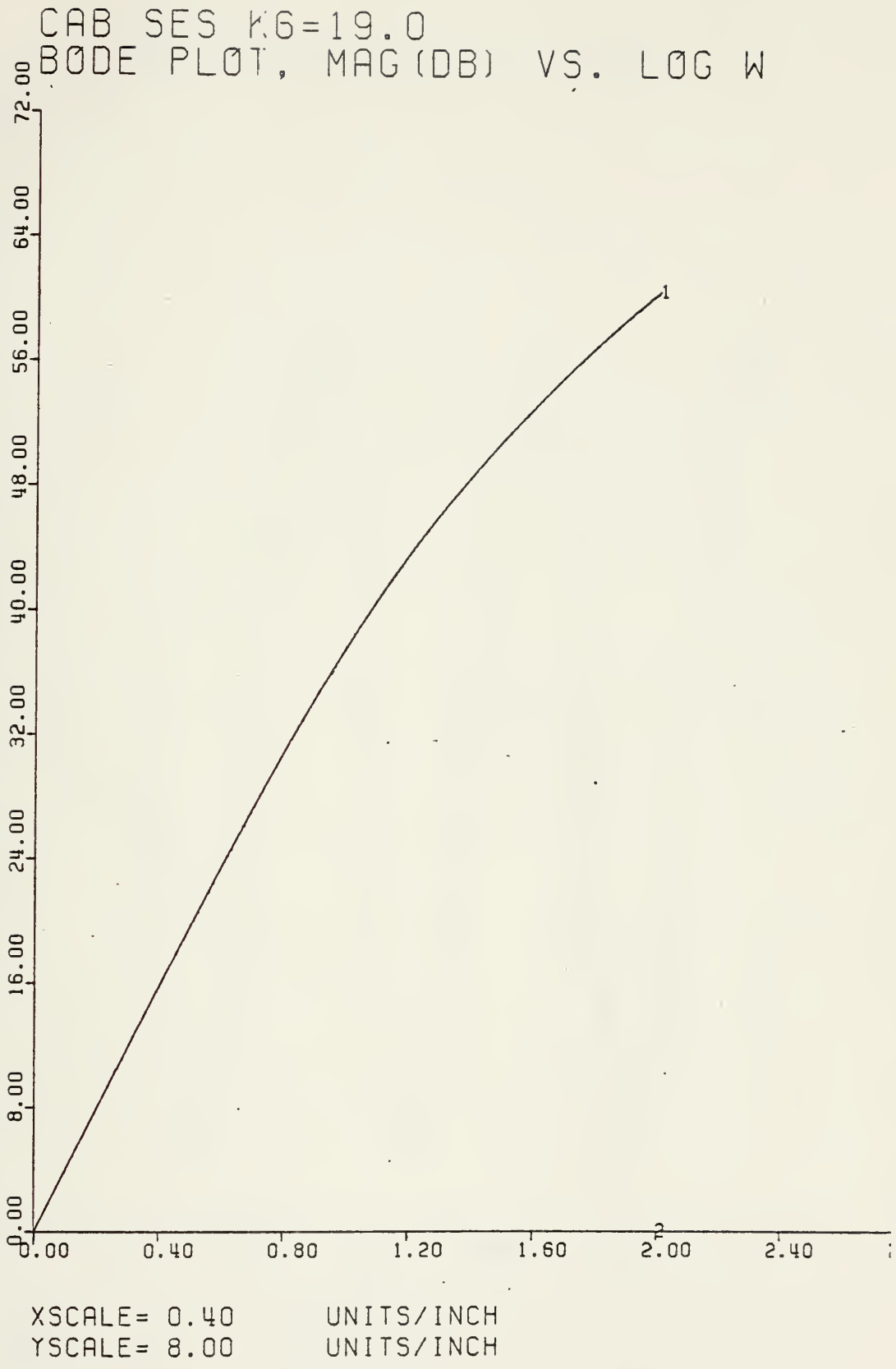
CAB SES KG=19.0
BODE PLOT, MAG(DB) VS. LOG W
72.00
64.00
56.00
48.00
40.00
32.00
24.00
16.00
8.00
0.00
0.00
0.40
0.80
1.20
1.60
2.00
2.40
1
2
XSCALE= 0.40 UNITS/INCH
YSCALE= 8.00 UNITS/INCH

Fiugre E6

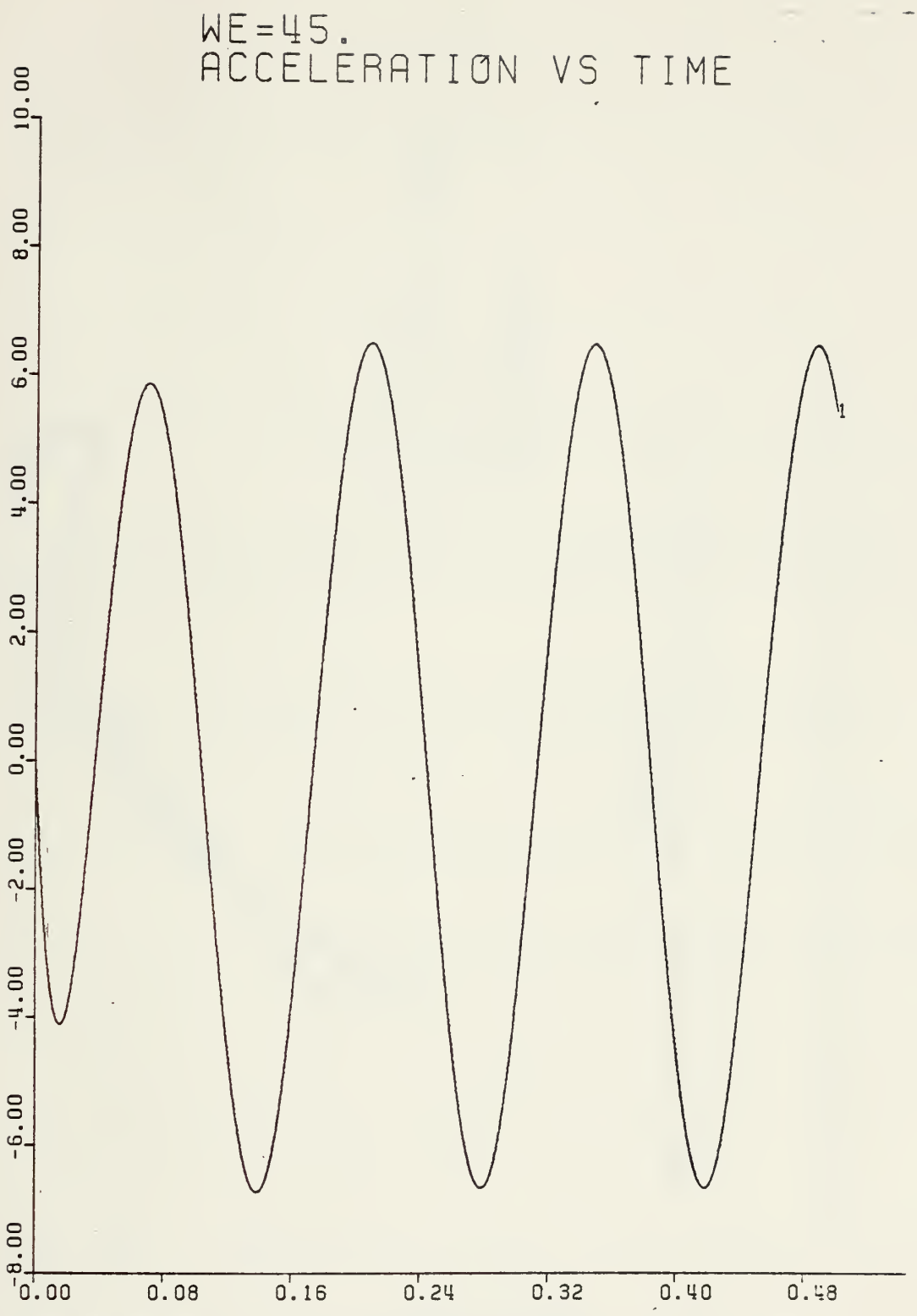
WE=45.
ACCELERATION VS TIME
10.00
8.00
6.00
4.00
2.00
0.00
-2.00
-4.00
-6.00
-8.00
0.00
0.08
0.16
0.24
0.32
0.40
0.48
XSCALE= 0.08 UNITS/INCH
YSCALE= 2.00 UNITS/INCH

Figure E7

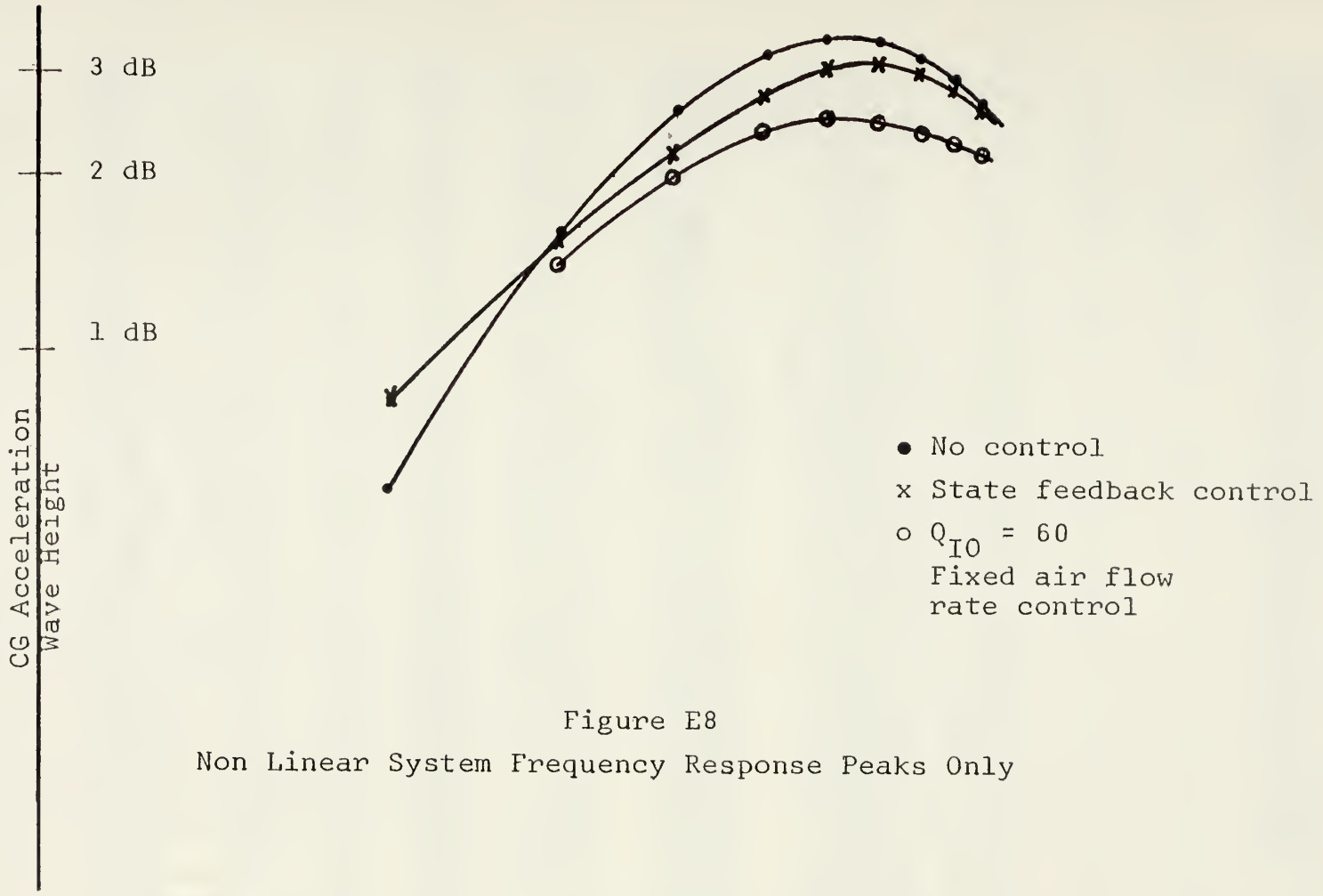

Figure E8

Non Linear System Frequency Response Peaks Only

LIST OF REFERENCES

1. Naval Postgraduate School Report NPS 62-78-008PR, Sensitivity Analysis of the XR-3 Heave Equations to Changes in Plenum Air Leakage and Influx Rates, by A. Gerba, Jr. and G. J. Thaler, September 1978.

2. The Society of Naval Architects and Marine Engineers, Naval Architecture, 1967.

3. Rohr Marine Inc., 3KSES Ship Control System Design Information Report, Vol. 1, 1978.

4. David W. Taylor Naval Research and Development Center Report, Vertical Plane Motions Response of an SES-100B Model, by R. S. Peterson and F. W. Wilson, January, 1978.

5. Menzel, R. F., Study of the Roll and Pitch Transients in Calm Water Using the Simulated Performance of the XR-3 Surface Effect Ship Loads and Motions Computer Program, M.S. Thesis, Naval Postgraduate School, Monterey, California, December 1975.

6. Boggio, J. M., A Study of Pressure Volume Rates and Plenum Membrane Additions to the Captured Air Bubble Surface Effect Ship, M.S. Thesis, Naval Postgraduate School, Monterey, California, 1976.

7. Grant, U. S., Jr., Study of Heave Acceleration/Velocity Control for the Surface Effect Ship, M.S. Thesis, Naval Postgraduate School, Monterey, California, 1974.

8. Booth, F. B., III, The Frequency Response and Operating Characteristics of the XR-3 Loads and Motions Program, M.S. Thesis, Naval Postgraduate School, 1976.

9. Figures 7, 8 and 9 are from an independent study by Major S. Carpenter conducted for Professor A. Gerba, Fall 1979.

10. Computer Programs for Computational Assistance in the Study of Linear Control Theory, James L. Melsa and Stephen K. Jones, McGraw-Hill, 1973.

11. DesJardins, B., A Users Manual for Linear Control Programs on the IBM/360, M.S. Thesis, Naval Postgraduate School, Monterey, California, 1979.

INITIAL DISTRIBUTION LIST

		No. Copies
1.	Defense Technical Information Center Cameron Station Alexandria, Virginia 22314	2
2.	Library, Code 0142 Naval Postgraduate School Monterey, California 93940	2
3.	Department Chairman, Code 62 Department Of Electrical Engineering Naval Postgraduate School Monterey, California 93940	1
4.	Professor Alex Gerba, Jr., Code 62Gz Department of Electrical Engineering Naval Postgraduate School Monterey, California 93940	5
5.	Professor George J. Thaler, Code 62Tr Department of Electrical Engineering Naval Postgraduate School Monterey, California 93940	5
6.	Professor D. M. Layton, Code 57Ln Department of Aeronautics Naval Postgraduate School Monterey, California 93940	1
7.	Surface Effects Ships Project Office PMS 304, Code 141 ATTN: Mr. H. Robertson P. O. Box 34401 Bethesda, Maryland 20034	6
8.	Lieutenant Dwight H. Everett, USN 197 Janine La Habra Heights, California 90631	1

Thesis
E7799
c.1

187578

Everett
Surface effect ship heave control using a linear regulator design.